The Plant Cell, Vol. 30: 889–906, April 2018, www.plantcell.org © 2018 ASPB.

OsALMT7 Maintains Panicle Size and Grain Yield in Rice by Mediating Malate Transport

Yueqin Heng,[a,1] Chuanyin Wu,[a,1] Yu Long,[c,1] Sheng Luo,[a] Jin Ma,[a] Jun Chen,[a] Jiafan Liu,[a] Huan Zhang,[b] Yulong Ren,[a] Min Wang,[a] Junjie Tan,[a] Shanshan Zhu,[a] Jiulin Wang,[a] Cailin Lei,[a] Xin Zhang,[a] Xiuping Guo,[a] Haiyang Wang,[a] Zhijun Cheng,[a,2] and Jianmin Wan[a,b,2]

[a] National Key Facility for Crop Gene Resources and Genetic Improvement, Institute of Crop Science, Chinese Academy of Agricultural Sciences, Beijing 100081, China
[b] State Key Laboratory for Crop Genetics and Germplasm Enhancement, Jiangsu Plant Gene Engineering Research Center, Nanjing Agricultural University, Nanjing 210095, China
[c] State Key Laboratory of Plant Physiology and Biochemistry, College of Biological Sciences, National Plant Gene Research Centre (Beijing), China Agricultural University, Beijing 100193, China

ORCID IDs: 0000-0001-7559-6660 (J.M.); 0000-0002-9032-3529 (Y.R.); 0000-0002-9983-1562 (J.T.); 0000-0003-4375-4892 (J.W.); 0000-0002-2519-4441 (X.Z.); 0000-0002-4936-7562 (X.G.); 0000-0002-1302-5747 (H.W.); 0000-0002-2768-8162 (Z.C.); 0000-0002-9307-5284 (J.W.)

Panicle size is a critical determinant of grain yield in rice (*Oryza sativa*) and other grain crops. During rice growth and development, spikelet abortion often occurs at either the top or the basal part of the panicle under unfavorable conditions, causing a reduction in fertile spikelet number and thus grain yield. In this study, we report the isolation and functional characterization of a panicle abortion mutant named *panicle apical abortion1-1* (*paab1-1*). *paab1-1* exhibits degeneration of spikelets on the apical portion of panicles during late stage of panicle development. Cellular and physiological analyses revealed that the apical spikelets in the *paab1-1* mutant undergo programmed cell death, accompanied by nuclear DNA fragmentation and accumulation of higher levels of H_2O_2 and malondialdehyde. Molecular cloning revealed that *paab1-1* harbors a mutation in *OsALMT7*, which encodes a putative aluminum-activated malate transporter (OsALMT7) localized to the plasma membrane, and is preferentially expressed in the vascular tissues of developing panicles. Consistent with a function for OsALMT7 as a malate transporter, the panicle of the *paab1-1* mutant contained less malate than the wild type, particularly at the apical portions, and injection of malate into the *paab1-1* panicle could alleviate the spikelet degeneration phenotype. Together, these results suggest that OsALMT7-mediated transport of malate into the apical portion of panicle is required for normal panicle development, thus highlighting a key role of malate in maintaining the sink size and grain yield in rice and probably other grain crops.

INTRODUCTION

Rice (*Oryza sativa*) is the major staple food for more than half of the world's population. Grain yield in rice is mainly determined by the number of panicles, number of grains per panicle, and grain weight, all of which are typical quantitative traits (Xing and Zhang, 2010). Panicle architecture, characterized by its size and branching pattern, determines the number of spikelets and, thus, the number of grains per panicle. Large panicles with more branches and spikelets (and, thus, higher grain number per panicle) have been preferred in breeding programs for new rice types with higher yield (Khush, 2000). Thus, understanding the molecular genetic mechanisms of panicle development and identification of superior alleles for large panicles are of great interest to both plant biologists and plant breeders.

The rice panicles are initiated following the switch from the vegetative to reproductive growth. At the transition, the shoot apical meristem is converted into an inflorescence meristem, which further initiates the primary branch meristems (BMs) and forms the main axis of the inflorescence. Subsequently, the primary BMs produce secondary BMs and spikelet meristems (SMs). SMs are also initiated from the secondary BMs and finally form spikelets (Ikeda et al., 2004; Tanaka et al., 2013). At maturity, rice panicle architecture, and thus the number of spikelets per panicle, is determined mainly by the length of the main axis and the length and number of primary and secondary branches. Over the past two decades, a number of genes regulating panicle development have been identified and functionally characterized. For example, *SMALL PANICLE*, *REDUCED CULM NUMBER1* (*RCN1*), *LAX PANICLE1* (*LAX1*), and *LAX2* are involved in the initiation of BMs and SMs (Nakagawa et al., 2002; Komatsu et al., 2003a; Oikawa and Kyozuka, 2009; Tabuchi et al., 2011). *ABERRANT PANICLE ORGANIZATION1* (*APO1*), *APO2*, and *TAWAW1* are involved in maintaining the identity of BMs by preventing precocious conversion of BMs to SMs (Ikeda et al., 2005, 2007; Ikeda-Kawakatsu et al., 2012; Yoshida et al., 2013). *FRIZZY PANICLE* is required to ensure initiation and identity of floral organs by

[1] These authors contributed equally to this work.
[2] Address correspondence to wanjianmin@caas.cn or chengzhijun@caas.cn.
The author responsible for distribution of materials integral to the findings presented in this article in accordance with the policy described in the Instructions for Authors (www.plantcell.org) is: Jianmin Wan (wanjianmin@caas.cn).
www.plantcell.org/cgi/doi/10.1105/tpc.17.00998

IN A NUTSHELL

Background: Rice is a staple food for more than half of the world's population. The number of spikelets on a panicle (panicle size) is an important component determining grain yield of a rice plant. The apical meristem initiates spikelet development after the transition from vegetative to reproductive growth. However, not all the spikelets develop to the mature stage to bloom, especially at the tip of the panicle, a phenomenon called panicle apical abortion (PAAB). It is known that imbalance in nutrition and environmental factors, such as high air temperature and high humidity, can cause severe PAAB, thus significantly reducing grain production. We have limited information on the molecular mechanisms involved in PAAB.

Question: We wanted to know if PAAB can be managed by either genetic engineering or agricultural practices. As a first step, we tried to understand mechanisms underlying PAAB.

Findings: We began with isolation of a PAAB rice mutant, *paab1-1*, that displays the panicle apical abortion phenotype. We cloned *paab1-1* and identified the causal gene as *OsALMT7*. The OsALMT7 protein is localized to the plasma membrane and functions as a malate transporter, with preferred expression in the phloem. Functional disruption of OsALMT7 in the mutant leads to graduated reduction in malate content from bottom to top of the panicle. Malate deficiency triggers programmed cell death, and as a result the spikelets with low malate content are finally aborted. Thus, OsALMT7 ensures a sufficient supply of malate to support rapid growth of the panicle, likely by loading the nutrient from the phloem. These findings highlight a key role of malate for maintaining panicle size and grain yield in rice.

Next steps: We would like to know if there is oscillation in OsALMT7 expression and malate content in developing panicles in response to changes of air temperature and humidity. As malate is a central metabolite in the plant cell, it will also be important to understand how malate deficiency triggers programmed cell death.

inhibiting the continued formation of axillary meristems from differentiated SMs (Komatsu et al., 2001, 2003b). Notably, the above genes encode different types of transcription factors. In addition, *GRAIN NUMBER1*, which encodes a cytokinin oxidase/dehydrogenase, regulates cytokinin accumulation in inflorescence meristems and plays an important role in determining the final number of SMs during panicle development (Ashikari et al., 2005). *DENSE AND ERECT PANICLE1* encodes a phosphatidylethanolamine binding protein-like domain protein that regulates meristematic activity and, thus, panicle morphology and grain number per panicle (Delhaize et al., 1993, 2007; Ashikari et al., 2005; Huang et al., 2009). Recently, miR156 was found to negatively regulate panicle branch number by downregulating the expression of *SQUAMOSA PROMOTER BINDING PROTEIN-LIKE14* (Jiao et al., 2010; Miura et al., 2010). Elucidating the functions of these genes and their regulatory relationships will contribute to breeding of new elite rice cultivars with "ideal" plant architecture and higher grain yield.

During rice growth and development, panicle abortion frequently occurs at either the top or basal parts of the panicle, particularly under unfavorable climatic conditions (malnutrition, extreme temperatures, shading, and water stress) (Senanayake et al., 1991; Saha et al., 1998; Yao et al., 2000; Kobayasi et al., 2001; Kato et al., 2008). Molecular genetic studies have identified several quantitative trait loci responsible for panicle apical abortion in rice (Cheng et al., 2011; Tan et al., 2011). In addition, a few genes involved in panicle degeneration have also been reported. *SHORT PANICLE1* was reported to control the spikelet abortion at the basal part of panicles, likely through regulating nitrate transport (Li et al., 2009). *ABERRANT SPIKELET AND PANICLE1* encodes a TOPLESS-related transcriptional corepressor; its loss-of-function mutant exhibits pleiotropic phenotypes including spikelet abortion at the middle and basal portions of panicle (Yoshida et al., 2012). Mutation in *TUTOU1*, which encodes a SCAR-like protein modulating actin organization, causes a pleiotropic phenotype including panicle apical abortion (Bai et al., 2015). Despite this progress, the molecular and genetic mechanisms underlying panicle abortion are still poorly understood.

In this study, we report the isolation and characterization of a spikelet abortion mutant named *panicle apical abortion1-1* (*paab1-1*) that exhibits degeneration of spikelets at the tops of panicles during the late stage of panicle development. Our data suggest that *OsALMT7* (an aluminum-activated malate transporter) is responsible for panicle apical abortion in *paab1-1* and plays an essential role in maintaining panicle size and grain yield by mediating malate transport in rice.

RESULTS

paab1-1 Exhibits an Apical Abortion Phenotype during Late Panicle Development

To understand the genetic and molecular mechanism underlying panicle development in rice, we identified a mutant, named *panicle apical abortion1-1*, from a tissue culture-derived population of the *japonica* rice cv Kitaake. The *paab1-1* mutant plants were morphologically similar to the wild type before the heading stage but showed severely aborted spikelets at the apical portion of each panicle at the heading stage (Figures 1A and 1B). The spikelet abortion rate, as the percentage of aborted spikelets in a panicle, was ~22% on average, and as a result, the number of grains per mature panicle dropped by ~20%

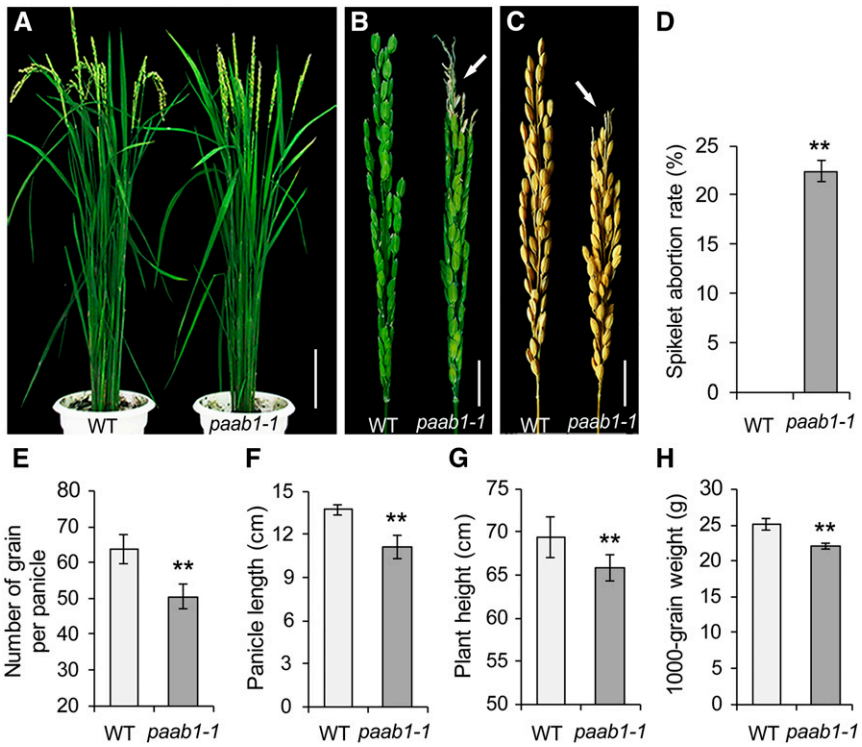

Figure 1. Phenotypic Chatracterization of *paab1-1*.

(A) Gross morphology of an adult *paab1-1* plant, showing the erect panicles due to aborted spikelets at the top as compared with the wild type (WT).
(B) A representative *paab1-1* panicle showing the aborted apical portion. The arrow indicates the degenerated spikelets.
(C) Comparison of a representative *paab1-1* mature panicle with the wild type, showing reduced panicle length due to the aborted tip in *paab1-1*.
(D) to **(H)** Comparison of spikelet abortion rate **(D)**, number of grain per panicle **(E)**, panicle length **(F)**, plant height **(G)**, and 1000-grain weight **(H)** between the wild type and *paab1-1*. All data shown are mean ± SE (n = 15). Asterisks represent statistically significant differences from the wild type, as determined by Student's t test. **P < 0.01.
Bars = 10 cm in **(A)** and 2 cm in **(B)** and **(C)**.

compared with the wild type (Figures 1C to 1E). In addition, the plant height of the *paab1-1* mutant was slightly lower than the wild type, largely due to a reduction in panicle length (Figures 1F and 1G). Moreover, the overall grain weight per panicle was reduced in *paab1-1* (Figure 1H). A more detailed analysis based on dividing the *paab1-1* panicle into three portions indicated that the spikelets and grains of the middle portion were smaller, whereas the basal spikelets and grains were normal in size compared with the wild type (Supplemental Figures 1A to 1F). Thus, *paab1-1* is a typical spikelet abortion mutant with a significant reduction in the sink size and grain yield.

To investigate when the apical spikelet degeneration starts to occur during panicle development, we divided the developmental course for panicles into six stages according to the panicle length (~1, ~3, ~5, ~7, ~10, and ~13 cm) (Figures 2A to 2F). In the variety Kitaake, the 1-cm stage represents a tiny panicle that already has differentiated spikelets, whereas the panicle at the 13-cm stage has almost reached the final size, although it is still inside the flag leaf sheath (Figures 2A, 2F, and 2G). During the development of panicles, the size of the spikelets also increases and reaches a maximum at the 13-cm stage (Figures 2H to 2M). Parallel observations showed that there were no apparent differences in the color and size of the panicles, spikelets, and anthers between the wild-type and *paab1-1* plants until the 10-cm stage, but the apical spikelet degeneration phenotype became clearly visible at the 13-cm stage in *paab1-1* (Figures 2A to 2F and 2H to 2M), as indicated by the white and smaller spikelets and shrunk anthers (Supplemental Figures 2A and 2B). These aberrant spikelets became shriveled after heading, and finally aborted (Figure 2N). To define the developmental defect more precisely, we examined the spikelet morphology at early development stages by scanning electron microscopy. The scanning electron microscopy observations revealed no difference in floral primordia between *paab1-1* and the wild type (Supplemental Figures 3A to 3F). We then performed histological analysis on apical spikelets at late stages. The lemma, palea, lodicules, stamens, and pistil in a *paab1-1* spikelet all were morphologically similar to those in the wild type at the 10-cm stage (Supplemental Figures 4A, 4B, 4E, and 4F). However, the floral organs in *paab1-1*, but not in the wild type, collapsed as the apical spikelets developed further (Supplemental Figures 4C, 4D, 4G, and 4H). Thus, apical abortion

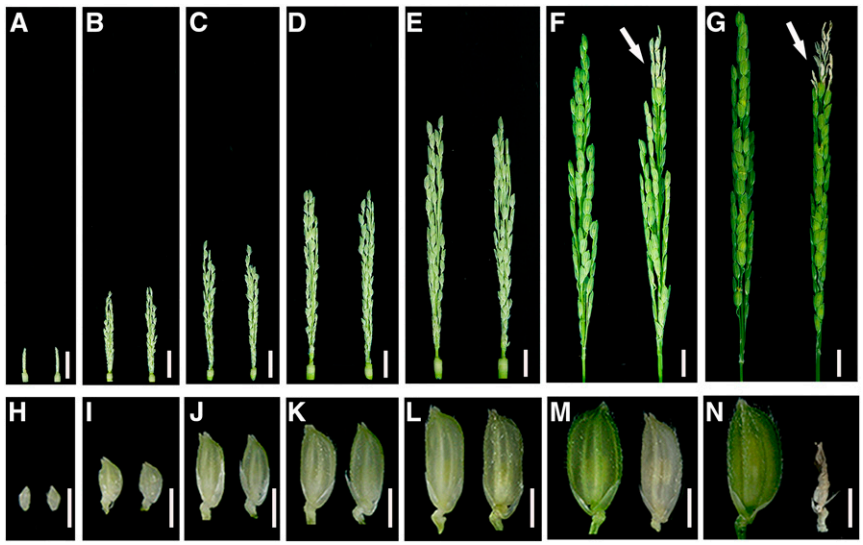

Figure 2. Degeneration of Top Spikelets Occurs at Late Stages of Panicle Development in *paab1-1*.

(A) to **(G)** Representative images of wild-type (left) and *paab1-1* (right) developing panicles, showing different stages as indicated by panicle length: 1 cm **(A)**, 3 cm **(B)**, 5 cm **(C)**, 7 cm **(D)**, 10 cm **(E)**, 13 cm **(F)**, and final size **(G)**. White arrows indicate the degenerating spikelets in **(F)** and **(G)**.
(H) to **(N)** Representative spikelets from the top of the corresponding panicles shown in **(A)** to **(G)**.
Note that degeneration of apical panicle becomes visible in *paab1-1* when the panicle reaches the 13-cm stage. Bars = 1 cm in **(A)** to **(G)** and 3 mm in **(H)** to **(N)**.

of the *paab1-1* panicle occurred during late panicle development (after 10 cm in length).

Cell Death Occurs in the Apical Spikelets of *paab1-1* Panicles

To further examine the cellular changes associated with the panicle apical abortion phenotype in *paab1-1*, we performed transmission electron microscopy (TEM) analysis of the apical spikelets at the 7-, 10-, and 13-cm stages, respectively. There were no obvious alterations in term of the organization and organelle content in *paab1-1* cells at the 7-cm stage, but less defined organelles with reduced contents were seen at the 10-cm stage. Breakdown of organelles was clear at the 13-cm stage compared with the wild type (Supplemental Figures 5A to 5F). Consistent with the findings from the TEM analysis, a terminal deoxynucleotidyl transferase-mediated dUTP nick-end labeling (TUNEL) assay, which detects nuclear DNA fragmentation, showed signals in *paab1-1* apical spikelet hull cells at the 10-cm stage (Figures 3B, 3I, and 3K), and the signals became more intense at the 13-cm stage (Figures 3C, 3M, and 3O). In addition, an electrophoresis analysis also showed clear DNA fragmentation in the aborted spikelets, further confirming that DNA degradation occurred in the aborted apical spikelets in *paab1-1* (Supplemental Figure 6). On the contrary, neither positive TUNEL signals nor obvious DNA fragments were detected in the wild-type spikelet cells of the corresponding stages (Figures 3D, 3F, 3H, 3J, 3L, and 3N). These results collectively suggest that cell degeneration in the *paab1-1* apical spikelets starts to occur between the 7- and 10-cm stages, before spikelet abortion becomes visible.

It has been well documented that excessive accumulation of H_2O_2 can trigger cell death (Van Breusegem and Dat, 2006). We therefore measured H_2O_2 content and found that there was a H_2O_2 blast in the *paab1-1* panicle at the 10-cm stage and that this change was located in the apical portion (Figures 3P and 3Q). High reactive oxygen species levels lead to oxidative damage of cellular components, such as membrane lipids; and malondialdehyde (MDA), an end product of lipid peroxidation, is regarded as an indicator of the production of reactive oxygen species (Chen and Murata, 2002). We measured the MDA content and found that MDA levels were elevated in the apical portions of 10- and 13-cm *paab1-1* panicles compared with the wild type (Figure 3R). We further examined the expression level of *OsVPE2* and *OsVPE3*, two representative genes associated with programmed cell death (PCD; Deng et al., 2011), and found that expression of *OsVPE2* was significantly increased in *paab1-1* at the 10-cm stage and even higher at the 13-cm stage, whereas a significant elevation was not seen until the 13-cm stage for *OsVPE3* (Figures 3S and 3T). Those results suggest that overaccumulation of H_2O_2 in the apical portion of the *paab1-1* panicle may trigger PCD at a stage not later than 10 cm in length.

Cloning and Characterization of the Causal Gene *OsALMT7*

To isolate the causal gene for the observed mutant phenotype, we constructed an F2 mapping population by crossing *paab1-1* with the *japonica* cultivar IRAT129. All the F1 individuals showed the panicle apical abortion phenotype, indicating that the mutation is dominant. We selected 1340 individuals with typical apical abortion from 2300 field-grown F2 plants to map

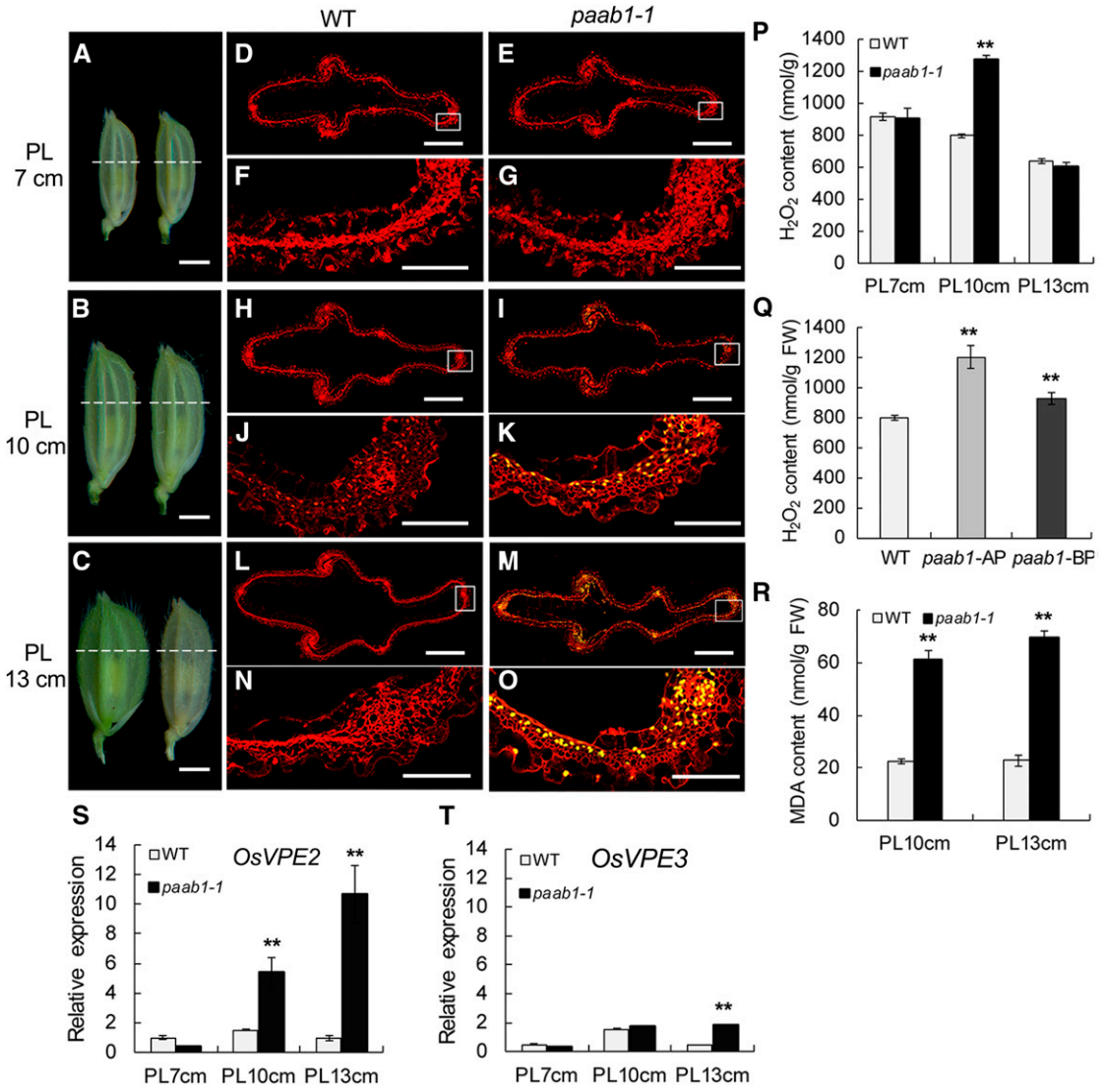

Figure 3. Cell Death-Related Events Are Triggered in *paab1-1*.

(A) to **(C)** Apical spikelets of the wild-type (left) and *paab1-1* (right) panicles at the 7-, 10-, and 13-cm stages (PL 7 cm, PL 10 cm, and PL 13 cm) were used for cell death analysis. The dotted white lines indicate the sites of cross sections for TUNEL assays.

(D) and **(E)** TUNEL assay of apical spikelet hull cells at the 7-cm stage. No DNA fragmentation signal was detected in both the wild type **(D)** and *paab1-1* **(E)**.

(F) and **(G)** Magnified views of the boxed areas in **(D)** and **(E)**, respectively.

(H) and **(I)** TUNEL assay of apical spikelet hull cells at the 10-cm stage. DNA fragmentation signal was detected in the *paab1-1* mutant **(H)**, but not in the wild type **(I)**.

(J) and **(K)** Magnified views of the boxed areas in **(H)** and **(I)**, respectively.

(L) and **(M)** TUNEL assay of apical spikelet hull cells at the 13-cm stage. There was no DNA fragmentation signal detected in the wild type **(L)**, but intensive signals were seen in *paab1-1* **(M)**.

(N) and **(O)** Magnified views of the boxed areas in **(L)** and **(M)**, respectively.

(P) Measurement of H_2O_2 content in panicles of the 7-, 10-, or 13-cm stages in the wild type and *paab1-1*, showing higher accumulation of H_2O_2 only at the 10-cm stage in *paab1-1*. The calculation was based on fresh weight of the whole panicles.

(Q) H_2O_2 content measurement in the wild-type panicles, compared with apical and lower portions of 10-cm young panicles of *paab1-1*. AP, apical portion; LP, lower portion; FW, fresh weight.

(R) Higher MDA content in the *paab1-1* apical spikelets at PL10 cm and PL13 cm.

(S) and **(T)** Expression level of *OsVPE2* **(S)** and *OsVPE3* **(T)** in the top regions of wild-type and *paab1-1* panicles at the 7-, 10-, or 13-cm stage, relative to the internal control (rice *UBIQUITIN* gene).

All data in **(P)** to **(T)** are presented as means ± SE of three independent biological replicates. $^{**}P < 0.01$, analyzed by the Student's *t* test compared with the wild type. Bars = 2 mm in **(A)** to **(C)**, 0.5 mm in **(D)**, **(E)**, **(H)**, **(I)**, **(L)**, and **(M)**, and 0.1 mm in **(F)**, **(G)**, **(J)**, **(K)**, **(N)**, and **(O)**.

paab1-1. The *paab1-1* locus was initially mapped to the long arm of chromosome 2 between the markers S2-10-3 and RM525. After fine mapping, the mutation was further narrowed down to an 82-kb genomic region between the markers C1 and H-4, in which nine open reading frames were annotated (Figure 4A). Sequence comparison between *paab1-1* and the wild type revealed a single nucleotide substitution of A to G in the predicted splicing site between the second intron and the third exon of LOC_Os02g45160 (referred to hereafter as *OsALMT7*; Liu et al., 2017) (Figure 4B). Consistent with the expected defect in splicing of the second intron, RT-PCR analysis detected two transcripts in the *paab1-1* mutant. One was 157 bp longer than that in the wild type due to retention of the second intron. In addition, a smaller transcript caused by alternative splicing of the second intron was detected (Figures 4B and 4C). Both transcripts detected in *paab1-1* had frame shifts starting from the Ala at position 164 and were terminated prematurely (Supplemental Figure 7). RT-qPCR analysis showed that *OsALMT7* is expressed at a higher level in the *paab1-1* mutant than in the wild-type plants (Supplemental Figure 8).

To verify whether the mutation of *OsALMT7* is responsible for panicle apical abortion in *paab1-1*, a 6-kb genomic fragment isolated from *paab1-1*, including the entire coding region of LOC_Os02g45160 and its flanking sequences, was introduced into the wild type. All 22 positive transformants (T_0) displayed the typical panicle apical abortion phenotype, mimicking the *paab1-1* phenotype (Figures 4D and 4E). This observation confirmed the identity of *OsALMT7* for panicle apical abortion

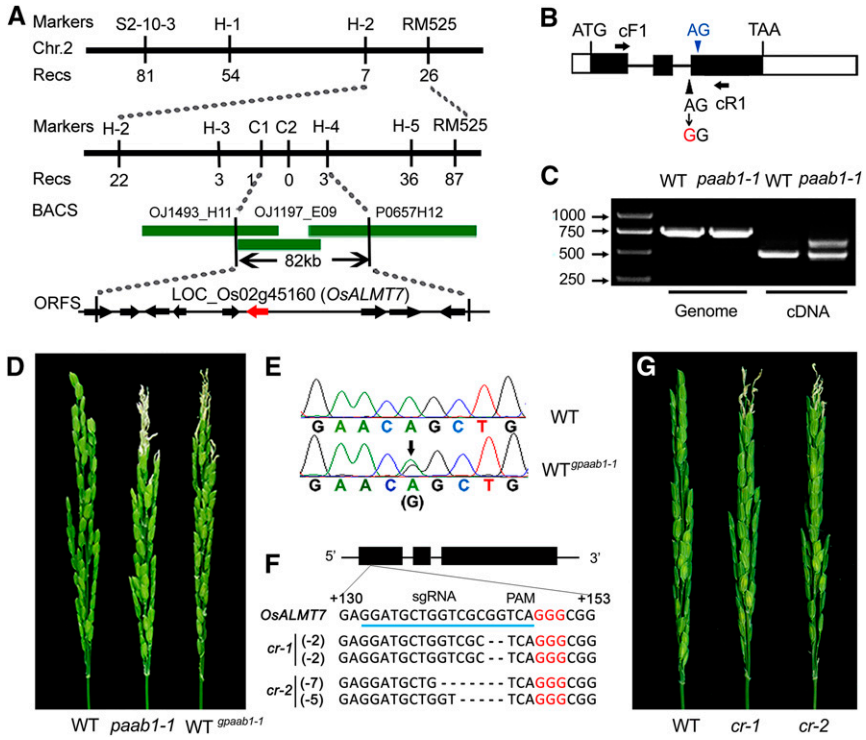

Figure 4. Map-Based Cloning of *paab1-1*.

(A) Fine mapping of *paab1-1*. The molecular markers and numbers of recombinants are indicated above and below the filled bars, respectively. The candidate open reading frame is highlighted in red.

(B) Genomic structure of the LOC_Os02g45160 (*OsALMT7*) gene. The white and filled boxes indicate untranslated regions and exons, respectively, and the black lines indicate introns. A base substitution in *paab1-1* is highlighted in red and an alternative splicing site in blue. cF1 and cR1 are a pair of primers for PCR analysis in **(C)**.

(C) RT-PCR analysis showing the presence of two abnormally sized transcripts in *paab1-1*. The larger transcript contains the 2nd intron due to mutation of the splicing site. The slightly smaller transcript is caused by the utilization of an alternative downstream splicing site as indicated by green in **(B)**. The genomic DNA was used as a control.

(D) Genetic confirmation of the *OsALMT7* gene. Wild-type plants transformed with a genomic fragment with the base substitution amplified from *paab1* ($WT^{gpaab1-1}$) resembled the *paab1-1* plants.

(E) Verification of coexistence of the wild type and mutated *OsALMT7* in the $WT^{gpaab1-1}$ plants by sequencing.

(F) Deletion mutation at the target site in two representative knockout lines generated by the CRISPR/Cas9 technology. The *cr-1* plant is a homozygous mutant carrying a 2-bp deletion on both homochromosomes and *cr-2* is a biallelic mutant carrying a 5-bp deletion on one chromosome and a 7-bp deletion on another. The filled bars indicate exons and lines indicate introns of *OsALMT7*. The sgRNA target sequence is underlined in blue and the PAM motif is highlighted in red letters.

(G) Representative panicles of knockout mutants showing the apical abortion phenotype.

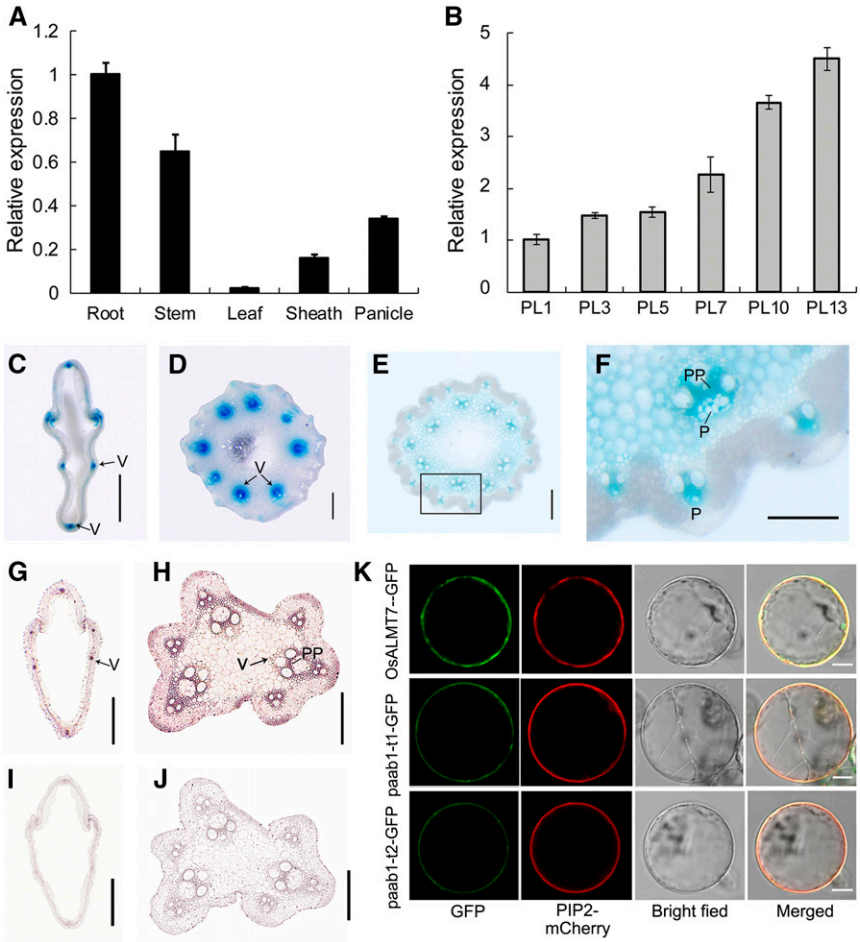

Figure 5. Expression Pattern and Subcellular Localization of the OsALMT7 Protein.

(A) Relative expression of *OsALMT7* in various tissues, including root, stem, leaf blade, leaf sheath, and panicle at the 7-cm stage (PL7). Rice *UBIQUITIN* was used as an internal control. Data are presented as mean ± SE (n = 3).

(B) Relative expression of *OsALMT7* in developing panicles at the 1-, 3-, 5-, 7-, 10-, and 13-cm stages (PL1 to PL13) before heading. Rice *UBIQUITIN* was used as an internal control. Data are presented as mean ± SE (n = 3).

(C) to **(F)** Promoter activity of *OsALMT7* as shown by GUS staining. Vascular tissue-preferred expression was seen in spikelet hull **(C)** and rachises at basal **(D)** and middle **(E)** parts of the panicles carrying the *OsALMT7-GUS* fusion. The squared area in **(E)** was magnified to show a vascular tissue **(F)**. P, phloem; PP, phloem parenchyma cells. Bars = 0.5 mm in **(C)**, 0.2 mm in **(D)** and **(E)**, and 0.1 mm in **(F)**.

(G) to **(J)** mRNA in situ hybridization of *OsALMT7* on transverse sections of panicle spikelet hull **(F)** and rachis **(G)**. Abundant *OsALMT7* transcripts were detected in vascular tissues of the panicle. *OsALMT7* sense probe was used as a negative control **(I)** and **(J)**. V, vascular tissue; PP, phloem parenchyma cells. Bars = 0.5 mm in **(G)** and **(I)** and 0.2 mm in **(H)** and **(J)**.

(K) Plasma membrane localization of OsALMT7 in rice protoplasts. The OsALMT7-GFP fusion protein was transiently coexpressed with PIP2-mCherry, a plasma membrane marker in rice protoplasts (upper row). cDNAs corresponding to the two mutant versions of transcripts detected in *paab1-1* were also fused to *GFP* (paab1-t1-GFP and paab1-t2-GFP) and coexpressed with PIP2-mCherry in rice protoplasts (middle and lower rows). From left to right: image of GFP (green), mCherry (red), protoplast, and merged GFP and mCherry. Bars = 5 μm.

and verified the dominant nature of the *OsALMT7* mutation in *paab1-1*. In addition, we isolated an allelic mutant, named *paab1-2*, which carried a point mutant in the third exon of *OsALMT7* (resulting an amino acid change from Ala to Phe at position 195) and displayed a similar panicle apical abortion phenotype to *paab1-1* (Supplemental Figures 7, 9A, and 9B). We also transformed a CRISPR-*Cas9* construct targeting the first exon of *OsALMT7* into the wild type (Kitaake) and identified 48 knockout plants (with frame shift). Strikingly, all the knockout plants exhibited the apical panicle abortion phenotype (Figures 4F and 4G). Similarly, RNA interference (RNAi) knockdown plants of *OsALMT7* in four *japonica* variety backgrounds (Kittake, Zhonghua 11, Asominori, and Nipponbare) all exhibited the apical panicle abortion phenotype (Supplemental Figures 10A to 10H). RT-qPCR analysis showed that expression of *OsALMT7*, but not that of its two closest homologs

OsALMT8 and *OsALMT9*, was significantly downregulated in the RNAi plants (Supplemental Figures 11A and 11B). Collectively, these results demonstrate that the mutation in *OsALMT7* is responsible for panicle apical abortion and that the mutant phenotype observed in *paab1-1* is likely caused by a dominant-negative mutation.

The predicted OsALMT7 protein consists of 488 amino acid residues and contains a conserved ALMT domain. Secondary structure prediction showed that OsALMT7 has seven potential transmembrane helices (Supplemental Figures 12A to 12C). BLAST searches of databases revealed that there are a number of ALMT orthologous proteins in land plants and that the rice ALMT family includes nine members. Phylogenetic analysis indicated that OsALMT7 is most closely related to AtALMT10 (with 45.6% amino acid identity), an uncharacterized Arabidopsis family member, but is more distantly related to other functionally characterized members, such as AtALMT1 (30.6% identity), AtALMT6 (22.2%), AtALMT9 (24.8%), AtALMT12 (26%), and TaALMT1 (37.4%) (Supplemental Figure 13). This bioinformatic information implies that OsALMT7 may execute a distinct function from those previously characterized homologs.

OsALMT7 Is Preferentially Expressed in Vascular Tissue and Localized to the Plasma Membrane

To elucidate the function of *OsALMT7*, we first analyzed the expression pattern of *OsALMT7* by RT-qPCR analysis. Expression of *OsALMT7* was detected in all rice organs analyzed, with relatively higher expression in the roots, stems, and panicles and lower expression in other organs including leaves and leaf sheathes (Figure 5A). A detailed analysis focusing on the panicle indicated that *OsALMT7* expression increased continuously during panicle development (Figure 5B). The expression pattern of *OsALMT7* was further evaluated in plants transformed with a GUS reporter gene driven by a 2614-bp promoter sequence of *OsALMT7*. We observed GUS activity in various organs examined, with the strongest staining in the roots, stems, and panicles and faint staining in leaves and leaf sheaths, similar to the RT-qPCR results (Supplemental Figures 14A to 14E). Since organ defects were observed only on the apical part of the panicle in *paab1-1*, we further analyzed *OsALMT7* expression in the panicle at the 10-cm stage. GUS staining in transverse sections of spikelet hulls and rachises of the panicle revealed strong promoter activity of *OsALMT7* in the vascular tissues (Figures 5C to 5E). A close-up observation showed that the GUS signals were mainly distributed in the phloem and phloem parenchyma cells of vascular tissues (Figure 5F). To verify this observation, an RNA in situ hybridization approach was employed. Strong signal was detected again in the vascular tissues of the spikelet hull and rachis (Figures 5G to 5J). The expression pattern of *OsALMT7* is consistent with its putative function as an anion transporter required for normal panicle development, likely involved in phloem loading of malate.

To test if OsALMT7 is localized to the plasma membrane as annotated (http://harrier.nagahama-i-bio.ac.jp/sosui/), *OsALMT7* was fused to the GFP reporter gene driven by the CaMV35S promoter. The resulting construct together with *PIP2*-mCherry, a plasma membrane marker (Lee et al., 2009), was transiently expressed in rice leaf sheath protoplasts. OsALMT7 was indeed colocalized with PIP2 on the plasma membrane in the protoplasts (Figure 5K). We also generated transgenic plants carrying the OsALMT7-GFP fusion protein transgene in the wild-type background. Plasma membrane localization was observed for OsALMT7-GFP fusion protein in the transgenic root cells (Supplemental Figures 15A to 15C). Notably, the predicted mutant products of *paab1-1* still retained the first five transmembrane helices (Supplemental Figure 7) and were also localized to the plasma membrane (Figure 5K). Moreover, OsALMT7-GFP was localized to the plasma membrane in plasmolyzed onion epidermal cells (Supplemental Figures 15D to 15G). To verify if the OsALMT7-GFP fusion protein was biologically functional, we cotransformed the CRISPR-*Cas9* construct together with an *OsALMT7′-GFP* fusion construct carrying synonymous base substitutions at the target site into the variety Zhonghua 11 (Supplemental Figure 16A). The knockout plants generated with the CRISPR-*Cas9* construct alone displayed panicle apical abortion, whereas all the 13 knockout (with frame shift in the internal *OsALMT7*) double transformants were normal in panicle development, suggesting that plasma membrane-localized OsALMT7′-GFP fusion protein is biologically functional (Supplemental Figures 16B to 16D).

OsALMT7 Functions as an Aluminum-Independent Malate Transporter

Several members of the ALMT family have been shown to function as anion channels and mediate malate transport (Barbier-Brygoo et al., 2011). To examine whether OsALMT7 exerts a similar biochemical function, an *OsALMT7* cDNA fragment was cloned into the vector pKK223-3 and then heterologously expressed in the *Escherichia coli* strain CBT315. CBT315 is a mutant strain defective in dicarboxylate transporter and is incapable of utilizing malate as the carbon source (Jeong et al., 2004). Growth of the transformed strain was partially restored on the M9 medium when malate was used as the sole carbon source, suggesting that OsALMT7 could mediate malate transport in *E. coli* (Figures 6A and 6B).

We further determined the electrophysiological properties of OsALMT7 by heterologously expressing it in *Xenopus laevis* oocytes. The two-electrode voltage clamp method was used to measure OsALMT7-mediated malate current in oocytes (Wagner et al., 2000). We observed that larger inward currents (anion efflux) appeared in the oocytes injected with the wild-type *OsALMT7*-cRNA than in the control oocytes injected with water or either of the two mutant cRNAs corresponding to the transcripts detected in *paab1-1* (*paab1-t1* or *paab1-t2*) and that the differences were greater when the oocytes were preloaded with malate than with water (Figures 6C to 6E). Moreover, the degree of enhanced inward currents by preloading of malate was concentration dependent (Figures 6F and 6G). In a separate assay where malate was added in the bathing solution, greater outward current (anion influx) was detected from the oocytes expressing *OsALMT7* than from those expressing *paab1-t1* or *paab1-t2* or from the control cells injected with water only (Figures 7A and 7B). Reversal potential measurements in oocytes expressing *OsALMT7* showed that increasing malate concentration in bath lead to negative shifts in the reversal

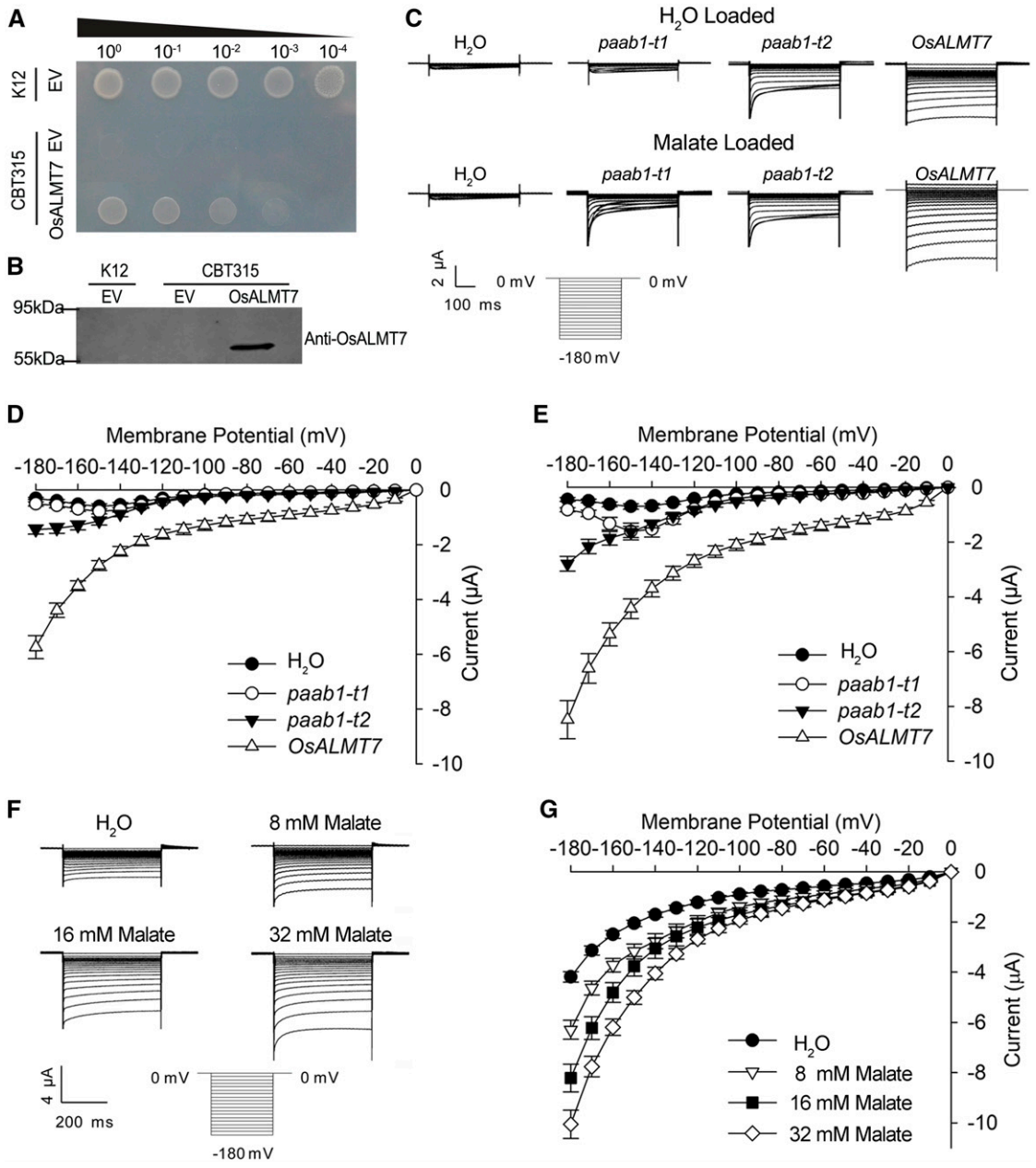

Figure 6. sALMT7 Mediates Malate Transport in *E. coli* and *X. laevis* Oocytes Systems.

(A) and **(B)** Partial suppression of the growth defect of the *E. coli* dicarboxylate transporter mutant CBT315 by expression of OsALMT7. CBT315 transfected with the empty vector (EV) or the *OsALMT7* gene (OsALMT7) and its wild type (K12) transfected with the EV only were grown on M9 agar medium with 10 mM malate (pH 6.6) as the sole carbon source. From left to right: transfected cells without dilution (10^0), diluted by 10× (10^{-1}), 100× (10^{-2}), 1000× (10^{-3}), or 10,000× (10^{-4}). Pictures were taken 3 d after inoculation. Immunoblot analysis showing the expression of the OsALMT7 protein in CBT315 is in **(B)**.
(C) Current recordings in *X. laevis* oocytes expressing *OsALMT7* and the *paab1-1* mutants. Whole-cell currents were recorded in oocytes injected with different cRNAs: *OsALMT7*, *paab1-t1*, *paab1-t2*, and with water as a control. The oocytes were preloaded with either water (upper panel) or malate (bottom panel). The holding potential was set to 0 mV and voltage protocols, as well as time and current scale bars for the recordings, are shown. *paab1-t1* and *paab1-t2* represent two cDNAs corresponding the two mutant versions of transcripts detected in *paab1-1*.
(D) and **(E)** The current-voltage (I-V) relationship of the steady state currents in oocytes preloaded with water **(D)** or malate **(E)**. The data are derived from the current recordings as those shown in **(C)** and presented as mean ± SE (n = 10 for each cRNA).
(F) OsALMT7-mediated currents recorded from *X. laevis* oocytes preloaded with a range of malate concentrations. Whole-cell currents were recorded in oocytes expressing *OsALMT7* at different intracellular malate concentrations (8, 16, and 32 mM). The oocytes preloaded with water were used as a control. The holding potential was set to 0 mV and voltage pluses were stepped between −180 mV and 0 mV in 10-mV increments. The time and current scale bars for the recordings are shown.
(G) The current-voltage (I-V) relationship of the steady state currents in oocytes with different intracellular malate concentrations. The data are derived from the current recordings as those shown in **(F)** and presented as mean ± SE (n = 10 for each malate concentration).

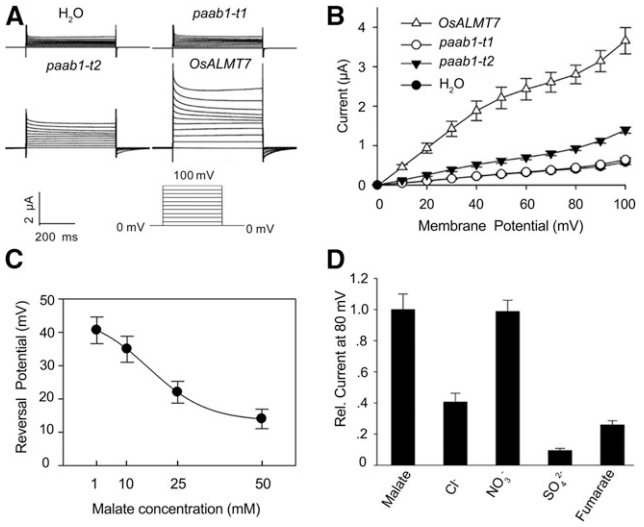

Figure 7. OsALMT7-Mediated Outward Currents and Anion Selectivity of OsALMT7 in *X. laevis* Oocytes.

(A) Recordings of OsALMT7-mediated outward currents in *X. laevis* oocytes. Whole-cell currents were recorded in oocytes injected with different cRNAs: *OsALMT7*, *paab1-t1* and *paab1-t2*, and with H_2O as a control. The outside solution was added with malate at a final concentration of 25 mM. The holding potential was set to 0 mV and voltage protocols, as well as time and current scale bars for the recordings are shown.

(B) The current-voltage (I-V) relationship of the steady state outward currents in oocytes. The data are derived from the current recordings as those shown in **(A)** and presented as mean ± SE (*n* = 15 for each cRNA).

(C) Reversal potential of *OsALMT7*-expressing oocytes preloaded with 46 nL of 100 mM malate was recorded in bath solutions with 1, 10, 25 or 50 mM malate. The reversal potential was valued through cross points of the I-V curves and *X*-axes (I=0). The data are presented as mean ± SE (*n* = 12 for each concentration).

(D) Anion selectivity of OsALMT7 in *X. laevis* oocytes. The outside solution was added with Cl^-, NO_3^-, SO_4^{2-} or fumarate, and with malate as a control. The relative current is the D-value from *OsALMT7*-expressing oocytes subtracted with that from control oocytes. Current for malate was set to 1. Calculation was based on currents measured at 80 mV only. The data are presented as mean ± SE (*n* = 10 for each anion).

potential (Figure 7C), which is indicative of malate permeation. Since inward current was recorded at hyperpolarization membrane potential and outward current was recorded at depolarization membrane potential, inside-out single channel current was recorded in oocytes to detect the directivity of OsALMT7 in oocytes. As shown in Supplemental Figure 17, at 180 mV command voltage, which means −180 mV membrane potential in the plasma membrane, inward currents were detected showing the efflux of malate. Furthermore, at −60 mV command voltage, which means 60 mV membrane potential in the plasma membrane, outward currents were detected showing the influx of malate. Taken together, these results confirmed that OsALMT7 functions as an anion channel capable of mediating transport of malate across the membrane. As ion channels are well known to form oligomers to perform transport activity (Middleton et al., 1996; Xicluna et al., 2007) and the predicted protein product of *paab1-1* is localized to the plasma membrane like the wild-type protein, we speculated that the truncated mutant protein may interfere with the normal function of the wild-type protein, thus causing a dominant-negative effect at a posttranslational level.

In addition to malate, some ALMT transporters were reported to translocate other organic anions such as fumarate or inorganic anions such as Cl^-, NO_3^-, and SO_4^{2-} (Kovermann et al., 2007; Piñeros et al., 2008a, 2008b). To examine the selectivity of OsALMT7 between malate and other anions, we replaced malate with fumarate, chloride, nitrate, or sulfate in the bathing solution and measured the corresponding outward currents in oocytes. The oocytes injected with *OsALMT7*-cRNA were permeable to fumarate, nitrate, chloride, or sulfate relative to the control injected with water, and the permeability to nitrate and malate was similar, as indicated by the outward currents (Figure 7D; Supplemental Figures 18A to 18C). Thus, OsALMT71 may also transport other anions in addition to malate, at least in *X. laevis* oocytes.

Several members of the ALMT family are involved in aluminum (Al) tolerance by mediating malate exudation from roots to soil (Sasaki et al., 2004; Hoekenga et al., 2006; Ye et al., 2017). To test whether OsALMT7 is involved in Al tolerance, we first tested if Al enhances the OsALMT7-mediated malate transport in the two-electrode voltage clamp assay. The addition of Al to the bathing solution had no significant effect on the inward currents in the oocytes preloaded with malate and injected with different versions of *OsALMT7*-cRNAs (Supplemental Figures 19A and 19B). Next, we treated rice seedlings with Al and found that the *paab1-1* plants had similar sensitivity as the wild type (Supplemental Figure 20A). In addition, our RT-qPCR analysis indicated that *OsALMT7* expression was not induced by Al (Supplemental Figure 20B). These results together suggest that OsALMT7 is an aluminum-independent malate transporter and is not associated with Al tolerance.

paab1-1 Is Defective in Malate Transport in the Apical Spikelets

Since OsALMT7 functions as a malate transporter, we next investigated if the apical spikelet abortion in *paab1-1* is associated with any change in malate level. Our malate content analysis indicated that there was a significant drop in the malate level of the panicle, but not of the root, stem, and leaf blade of *paab1-1*, compared with the wild type (Figure 8A). More detailed analysis revealed that malate content started to decrease in the apical portion at the 7-cm stage, and the decrease became more dramatic and extended to the middle portion during further panicle development, but no significant differences were detected in the lower portion of panicle between *paab1-1* and the wild type (Figure 8B). No difference in nitrate level was detected between *paab1-1* and the wild type (Supplemental Figure 21), suggesting that other transporters might be responsible for transporting nitrate in the panicle of *paab1-1*. To further investigate if malate transport is impaired in other tissues of *paab1-1*, we grew rice seedlings in a hydroponic solution supplemented with 0.3 mM malate for 24 h and measured the malate content in the roots and shoots. The malate content was lower in the shoots but not in the roots of

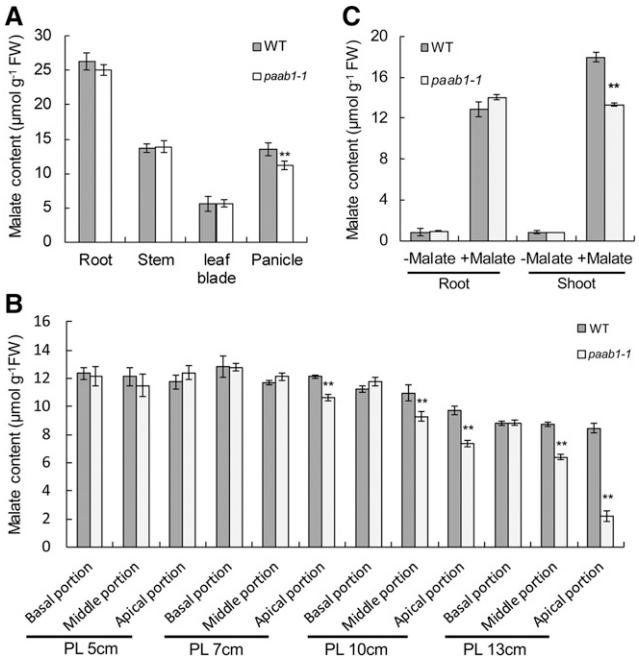

Figure 8. Malate Content Is Decreased in the *paab1-1* Panicle.

(A) Malate content in the indicated tissues sampled from field plants at the PL10 cm stage. Whole panicles were used for this analysis.
(B) Malate content in different panicle portions at different developmental stages. The panicle was divided into basal, middle, and apical portions to measure gradients in changes of malate content.
(C) Malate transport assay in seedlings grown in hydroponic solution. Five-day-old rice seedlings were exposed to the hydroponic solution added with 0 or 0.3 mM malate for 24 h before sampling.
All data are presented as means ± SE ($n = 3$) of three independent biological replicates. Asterisks above bars indicate significant difference from the wild type (**P < 0.01) analyzed by the Student's *t* test.

paab1-1, compared with the wild type (Figure 8C). This result implies that transport of malate might be impaired in *paab1-1*, thus causing spikelet degeneration in the apical portion of panicle.

Injection of Malate into Developing Panicles Alleviates Apical Spikelet Degeneration in *paab1-1*

To further test the notion that decreased malate might be the trigger for apical panicle abortion in *paab1-1*, we first injected a top site of the wild-type panicle at approximately the 7-cm stage with water or with 1.5 mM malate and observed that the injections did not pose any visible injury or phenotypic change to the subsequent growth of the panicles (Supplemental Figures 22A to 22C). Then we injected 1.5 mM malate into the *paab1-1* panicles at a similar stage. The *paab1-1* plants injected at this stage still developed aborted apical spikelets, not different from the control injected with water only (Supplemental Figures 22D and 22E). When 3 mM malate was injected into younger *paab1-1* plants with panicles of ~5 cm in length, however, the apical spikelet abortion phenotype was alleviated significantly (Figures 9A to 9C and 9H). Increase of malate concentration to 6 mM further rescued the apical spikelets in *paab1-1* (Figures 9D and 9H). A second injection 4 d after the first had a mild improvement in maintaining the panicle growth in *paab1-1* (Figures 9E to 9G and 9I). Together, those results support the conclusion that malate deficiency is the underlying cause of spikelet apical degeneration in *paab1-1*.

DISCUSSION

Panicle Apical Abortion in *paab1-1* Reduces Panicle Size and Is Accompanied by Programmed Cell Death

Panicle abortion is a widespread physiological defect that reduces grain yield in rice and other cereal crops (Sheehy et al., 2001; Yamagishi et al., 2004). However, the genetic and molecular mechanisms governing panicle abortion have remained poorly characterized. In this study, we isolated a new panicle abortion mutant named *paab1-1*, which exhibits spikelet degeneration at the apical portion of panicle, and consequently a severe reduction in panicle size and grain yield (Figures 1B and 1E). In addition, growth of spikelets in the middle portion of *paab1-1* panicle is also affected, resulting in reduced grain size (Supplemental Figure 1).

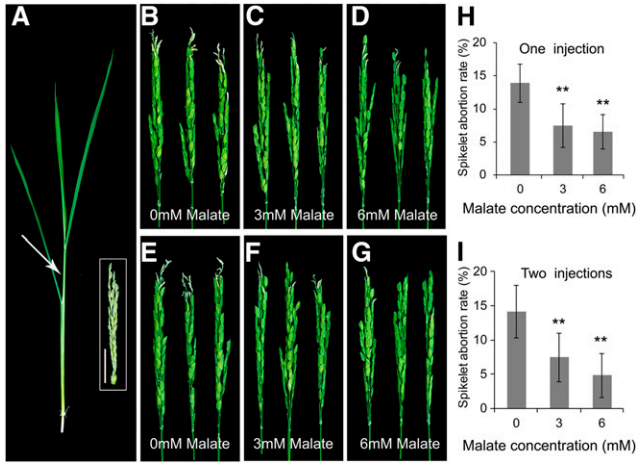

Figure 9. Injection of Malate to *paab1-1* Plants Alleviates Apical Panicle Abortion.

(A) A representative tiller, with the panicle at about the 5-cm stage, used for malate injection. Arrow indicates an approximate injection site. The dissected panicle is shown in the white box. Bar = 1 cm.
(B) to **(D)** Representative *paab1-1* panicles after injection with 0 (water control), 3, or 6 mM malate.
(E) to **(G)** Representative *paab1-1* panicles after two sequential injections with 0, 3, or 6 mM malate. The second injection was made 4 d after the first injection with the same malate concentrations.
(H) and **(I)** Spikelet abortion rate of *paab1-1* panicles injected with malate for one **(H)** or two sequential times **(I)**.
Photographs in **(B)** to **(G)** were taken after the panicles emerged out of the flag leaf sheaths. All data shown in **(H)** and **(I)** are mean ± SE ($n = 10$). Asterisks indicate significant difference from 0 mM malate, as determined by the Student's *t* test at P < 0.01.

Notably, the defects in both the apical and middle portions are observed after the panicles have already formed, suggesting that *OsALMT7* is required for maintaining the development of differentiated panicles. Detailed observation revealed that panicle abortion becomes visible at the stage of 10 cm in length (Figures 2F and 2M). Furthermore, we found that there is a H_2O_2 burst and increased MDA levels in the aborted spikelets, accompanied by organelle degeneration, DNA degradation, and enhanced PCD-related gene expression (Figure 3). Together, these results indicate that the phenotype of *paab1-1* is accompanied by programmed cell death in the apical spikelets.

OsALMT7 Encodes an ALMT Transporter Independent of Aluminum Activation

The family of aluminum-activated malate transporters has been shown to perform a range of physiological functions related to guard cell regulation, mineral nutrition transport, grain metabolism, and malate accumulation during tomato fruit ripening, besides being involved in aluminum tolerance (Hoekenga et al., 2006; Piñeros et al., 2008b; Sasaki et al., 2010; Xu et al., 2015; Ye et al., 2017). For example, The *Arabidopsis thaliana* members AtALMT6 and AtALMT9 mediate malate currents across the vacuole and regulate stomata movement (Meyer et al., 2011; De Angeli et al., 2013). TaALMT1 and AtALMT1 have been reported to mediate malate excretion from the plasma membrane of root cells into rhizosphere to form nontoxic complexes and detoxify Al^{3+} accumulation in soil (Sasaki et al., 2004; Hoekenga et al., 2006). In this study, we show that *OsALMT7* encodes an aluminum-activated malate transporter. The rice genome contains nine members of the ALMT family (Delhaize et al., 2007) and functional analysis has been reported for only one of these genes (Liu et al., 2017). Our phylogenetic analysis revealed that OsALMT7 belongs to the same clade as TaALMT1, AtALMT1, and ZmALMT1 (Supplemental Figure 13). However, in contrast with TaALMT1 and AtALMT1, we found that OsALMT7 can mediate transport of malate across the plasma membrane independent of Al^{3+} activation (Figures 6 and 7; Supplemental Figure 19). As most anion channels mediate anion transport depending on the membrane potential and anion concentration on both sides of the plasma membrane, and the membrane potential of most plant cells is negative (hyperpolarized potential) under normal physiological conditions, anion channels generally favor the function of anion efflux from the cytosol. However, some cells such as xylem cells show depolarized membrane potential in plants (Wegner and Zimmermann, 2004; Wegner et al., 2011). Given that OsALMT7 mediates large inward/outward currents in oocytes (Figures 6C to 6E, 7A and 7B), we speculate that OsALMT7 may mediate influx or efflux in spikelet cells on the panicle, depending on the membrane potential and cytosolic and extracellular malate concentration.

OsALMT7 Is Required for Malate Supply and Sustained Growth of the Panicle during Late Development Stages

Panicle outgrowth in rice is a rapid elongation process, accompanied by maturation of reproductive organs that must be supported by higher rates of nutrient and energy supply. As such, abortion of spikelets is often seen, particularly under unfavorable environmental conditions (Yao et al., 2000; Itoh et al., 2005; Smith and Stitt, 2007; Kato et al., 2008). In support of this notion, nitrogen nutrition has also been shown to be required for spikelet development on the panicle (Fu et al., 2011). In addition, the maize (*Zea mays*) *tassel-less1* mutant, which has a defect in boron transport and thus insufficient boron supply to the rapidly growing reproductive tissue and developing organs, shows a small and tip-barren ear phenotype (Durbak et al., 2014).

In this study, we demonstrated that malate is a key metabolite required to support sustained growth of the panicle during late development and that this process requires *OsALMT7* based on the following observations. First, we found that the accumulation of malate is reduced in the aborted portions of *paab1-1* panicles, compared with the apical portions of the wild type (Figure 8B). Second, we showed that injection of malate can effectively alleviate the aborted spikelets phenotype in *paab1-1* (Figure 9). Third, we found that OsALMT7 can mediate transport of malate across the plasma membrane independent of Al^{3+} activation (Figures 6 and 7; Supplemental Figure 19). As malate is a central metabolite in the plant cell, involved in the mitochondrial tricarboxylic acid (TCA) and glyoxylate cycles in plant species (Martinoia and Rentsch, 1994; Fernie and Martinoia, 2009; Sweetman et al., 2009), one possibility might be that a deficiency of malate exerts a negative influence on energy generation and storage, biosynthesis of intermediates in TCA and glyoxylate cycle, or cellular pH status, which in turn impair other cellular activities such as import of sucrose and other nutrients, nitrogen reduction, and photorespiration. Therefore, further investigation of *paab1-1* on expression level of TCA enzyme genes, content of TCA intermediates, nitrogen and sucrose level, and photorespiration activity may provide useful clues to understanding the link between low malate and PCD. Alternatively, the charge movement caused by uptake of anion uptake (in this case, malate) and the associated changes in electroneutrality or pH cannot be excluded. Moreover, it has been shown that malate protects plants from aluminum toxicity by its efflux from root cells to rhizosphere (Hoekenga et al., 2006) and that malate plays an important role in regulating guard cell aperture by maintaining cellular osmotic pressure in guard cells (Mathieu et al., 1986; Meyer et al., 2010). A recent study showed that altered expression of *OsALMT4* in rice disrupted the distribution of certain minerals including Mn and B nutrition (Liu et al., 2017). OsALMT7 might also play a role in regulating mineral nutrition balance in rice. Furthermore, as OsALMT7 is also permeable to nitrate and defects in nitrate transport have been shown to cause a small-panicle phenotype (Li et al., 2009), possible effects of OsALMT7 on these cellular processes and their relationship with panicle development remain to be investigated in future studies.

METHODS

Plant Materials and Growing Conditions

The *paab1-1* mutant was isolated from a tissue culture-derived population of the *japonica* cultivar Kitaake. The F2 mapping population was derived

from a cross between *paab1-1* and the *japonica* cultivar IRAT129. At the heading stage, F2 plants with the *paab1-1* phenotype were used for gene mapping. Rice (*Oryza sativa*) plants were grown in the experimental field at the Chinese Academy of Agricultural Sciences during the natural growing season. Transgenic plants were grown in pots in a greenhouse under standard growth conditions.

For aluminum treatment experiment, the wild-type and *paab1-1* seeds were soaked in water overnight at 30°C in the dark and then germinated on wet filter paper at 30°C for 2 d. The germinating seeds were transferred to a net floating on a 0.5 mM $CaCl_2$ solution (pH 4.5). After 3 d, the seedlings were exposed to the same solution but supplemented with 0, 50, or 100 μM $AlCl_3$ for 3 d. Sensitivity of the plants to Al was determined by measuring their root length. To examine whether Al has an effect on the expression level of *OsALMT7*, 6-d-old seedlings of the wild type and *paab1-1* were exposed to 0 or 50 μM $AlCl_3$ for 6 h. The roots and shoots treated with or without Al were harvested for RNA extraction.

TUNEL Assay

Apical spikelet hulls of the wild type and *paab1-1* at different developmental stages were collected and fixed in the FAA fixation solution (containing an 18:1:1[v/v] mixture of formalin, 70% ethanol, and acetic acid) for 24 h. The hulls were then dehydrated through an ethanol series (90, 70, and 50%) and embedded in paraffin (Sigma-Aldrich). Tissue cross sections (10 μm in thickness) were cut with a rotary microtome and hydrated through an ethanol series (100, 85, 70, and 50%) and treated with proteinase K in phosphate buffer (pH 7.4). The TUNEL assay was performed with a Dead End Fluorometric TUNEL Kit (Promega) according to the manufacturer's instructions. The green fluorescence of fluorescein (TUNEL signal) and red fluorescence of propidium iodide were analyzed at 488 nm (excitation) and 520 nm (detection), and 488 nm (excitation) and 610 nm (detection), respectively, under a confocal laser scanning microscope (LSM 700; Carl Zeiss).

Scanning Electron Microscopy and TEM

For scanning electron microscopy, flowers at different developmental stages were fixed in 2.5% glutaraldehyde and 0.1 M phosphate buffer at 4°C overnight. Following ethanol dehydration, samples were critical point dried, sputter coated with gold in an E-100 ion sputter, and observed using a scanning electron microscope (S3400N; Hitachi).

For TEM, apical spikelets of the wild type and *paab1-1* at different developmental stages (7, 10, and 13 cm in panicle length) were collected and fixed with 2.5% glutaraldehyde in a 0.1 M phosphate buffer at 4°C overnight. After being rinsed with 0.1 M phosphate buffer, they were incubated in a solution containing 1% (w/v) osmium tetraoxide for 4 h at room temperature. The samples were subsequently dehydrated through a graded series of ethanol and then embedded in acrylic resin (London Resin Company). Ultrathin sections (50–70 nm) were double stained with 2% (w/v) uranyl acetate and 2.6% (w/v) lead citrate aqueous solutions and observed with a JEM-1230 transmission electron microscope (JEOL) at 80 kV.

DNA Laddering Analysis

Apical spikelets of the wild type and *paab1-1* at different developmental stages (7, 10, and 13 cm) were collected and ground in liquid nitrogen. The DNA was exacted by the CTAB method as previously described (Dellaporta et al., 1983). Then, the DNA concentration was estimated using NanoDrop (ND-1000). For each sample, 2 μg DNA was loaded per lane and separated on a 2% (w/v) agarose gel by electrophoresis. Fragmented DNA was captured under UV light with a GEL Doc XR Imager.

Quantitative Measurement of H_2O_2 Content

H_2O_2 was extracted from panicles of different developmental stages according to the previously described method (Rao et al., 2000). Reactions for quantifying H_2O_2 content were performed using a hydrogen peroxide assay kit (Beyotime) according to the manufacturer's instructions. The H_2O_2 content was measured instantly with a spectrometer (SpectraMax Plus^{384}) at a wavelength of 560 nm. The measurements were performed in triplicate and the data were analyzed by the variance (ANOVA), and means were compared using a Student's *t* test.

MDA Content Analysis

MDA accumulation has been considered an indicator of lipid peroxidation and cell death (Hodges et al., 1999). For determination of MDA content, panicle samples (0.2 g fresh weight) were homogenized in 5 mL of phosphate buffer (pH 7.8) and centrifuged at 3,000*g* for 10 min. The supernatant was mixed with an equal volume of 5% (w/v) trichloroacetic acid containing 0.5% (w/v) thiobarbituric acid. The mixture was incubated at 95°C for 15 min and then immediately cooled in an ice bath. After centrifugation at 3,000*g* for 10 min, the absorbance of the supernatant was measured at 450, 532, and 600 nm, respectively. Finally, the MDA content was calculated according to the equation $6.45 \times (OD_{532} - OD_{600}) - 0.56 \times OD_{450}$ (Lin et al., 2012). The MDA content analysis was performed with three independent replicates on which five different plants were used.

Map-Based Cloning of *paab1-1*

Map-based cloning was performed using more than 1300 mutant individuals selected from the F2 mapping population. We first developed molecular markers according to sequence polymorphisms between Kitaake and IRAT129 including SSR, InDel, CAPS, and dCAPS. Primers used for generating those markers are listed in Supplemental Table 1. The *paab1-1* locus was mapped to an interval between the markers H-2 and RM525 on the long arm of chromosome 2. Fine mapping anchored the mutation site to an 82-kb genomic region between the markers C1 and H-4. This region spans the BAC clones OJ1493-H11, OJ1197-E09, and P0657H12. The primers used for amplifying the candidate gene LOC_Os02g45160 are listed in Supplemental Table 1.

Constructs for Complementation Test, RNAi, and CRISPR

For the genetic complementation test, a 6-kb genomic fragment covering the entire coding region of LOC_Os02g45160, plus 1705 bp upstream sequence and 997 bp downstream sequence, was amplified by PCR from *paab1-1* with the primer pair p2300-OsALMT7-F and p2300-OsALMT7-R and inserted into the binary vector pCAMBIA2300 using the restriction endonucleases *Sac*I and *Sal*I. To generate the *OsALMT7* RNAi construct, two inverted repeats of 325 bp were amplified from the wild type with the primer pair RNAi-F and RNAi-R. The PCR fragments were sequentially cloned into the pCUbi1390-ΔFAD2 vector in the sense and antisense orientations using the *Xho*I/*Kpn*I and *Bam*HI/*Xba*I sites to create the RNAi construct pUbi-dsRNAi OsALMT7. To create *OsALMT7* CRISPR lines, an 18-bp sgRNA targeting the first exon of *OsALMT7* was cloned into the CRISPR-*Cas9* expression vector according to the method previously described (Miao et al., 2013). The resulting construct was introduced into the Kitaake (wild type) by *Agrobacterium tumefaciens*-mediated transformation as described (Hiei and Komari, 2008). The primers for creating the above constructs are listed in Supplemental Table 2. The CRISPR transgenic plants were genotyped by PCR amplification and DNA sequencing.

RNA Extraction and RT-qPCR Analysis

Total rice RNA was extracted using a RNA prep pure kit (Zymo Research) and treated with DNaseI according to the manufacturer's instructions. The first-strand cDNA was synthesized from 2 μg of total RNA with oligo(dT) as the primer, using a reverse transcription kit (TaKaRa). Subsequently, the first-strand cDNA was used for PCR amplification with the primer pair cF1 and cR1 to detect unusual splicing caused by the base pair substitution mutation (Supplemental Table 2).

RT-qPCR was performed using ABI7500HT Fast real-time PCR system with the SYBR Premix Ex Taq (TaKaRa; RR041A), following the manufacturer's instructions. The rice *UBIQUITIN* gene was used as an internal control. Gene expression level was determined from three independent replicates, each consisting of five plants for tissue samples, and three technical replicates per tissue sample were analyzed. Gene-specific primers are shown in Supplemental Table 2.

GUS Staining Assay

For promoter activity analysis, a 2614-bp genomic fragment upstream of the ATG start codon was PCR-amplified from wild-type genomic DNA with the primer pair promoter-F and promoter-R (Supplemental Table 2) and fused to the GUS reporter gene in the binary vector pCAMBIA1305. The resulting construct *pOsALMT7* promoter-*GUS* was introduced into the wild type by the Agrobacterium-mediated transformation method. Histochemical staining of GUS activity in the transgenic plants was performed as previously described (Jefferson, 1987). Images were captured using Leica Application Suite 3.3.0 software.

Subcellular Localization of OsALMT7

To investigate the subcellular localization of OsALMT7, the coding sequence of *OsALMT7* was amplified with the primer pair pAN580-P1F and pAN580-P1R from the wild-type plant and then cloned into the pAN580 vector to generate an N-terminal fusion with GFP under control of the CaMV 35S promoter, resulting in the pAN580-OsALMT7-GFP construct. cDNAs corresponding to the two mutant versions of transcripts were amplified with the primer pairs (pAN580-P2F/pAN580-P2R and pAN580-P3F/pAN580-P3R; Supplemental Table 2) from *paab1-1* and cloned into pAN580, generating pAN580-paab1-t1-GFP and pAN580-paab1-t2-GFP, respectively. Each of those constructs was then transiently coexpressed with PIP2-mCherry, a plasma membrane marker, in rice protoplasts according to the protocol described previously (Bart et al., 2006; Lee et al., 2009). Stable transgenic plants carrying the *OsALMT7-GFP* fusion was also produced by the Agrobacterium-mediated method. *OsALMT7′-GFP* fusion construct was created with three synonymous base substitutions at the sgRNA targeted site and then was co-transformed into the variety Zhonghua 11 together with the *OsALMT7* CRISPR-*Cas9* construct. GFP fluorescence in the rice protoplasts and roots of transgenic plants was visualized with a confocal laser scanning microscope (LSM 700).

In addition, the construct pAN580-OsALMT7-GFP and the membrane marker were heterologously expressed in onion epidermal cells by the particle bombardment method (Bio-Rad PDS-1000) according to the protocol previously described (Von Arnim, 2007). To induce plasmolysis, cells were treated with 1 M mannitol for 15 min. The GFP signal in the epidermal cells was visualized with a confocal laser scanning microscope (LSM 700).

Phylogenetic Analysis of ALMT Proteins

Amino acid sequences homologous to OsALMT7 were downloaded from the National Center for Biotechnology Information website (http://blast.ncbi.nlm.nih.gov/). Multiple sequence alignments of these homologs (Supplemental Data Set 1) were performed using ClustalX 2.0 and the phylogenetic tree was constructed using the neighbor-joining method (MEGA5 software).

Complementation Test of OsALMT7 in *Escherichia coli*

Functional complementation test of OsALMT7 in *E. coli* was conducted according to the method described previously (Lee et al., 2008). The wild-type strain K12 (CGSC4401) and its dicarboxylate transport mutant strain CBT315 (CGSC5269) were obtained from The *E. coli* Genetic Resources Center at Yale University (http://cgsc.biology.yale.edu). The *OsALMT7* cDNA fragment was cloned into the *Eco*RI site of the pKK223-3 vector with the primer pair pkk223-OsALMT7-F and pkk223-OsALMT7-R (Supplemental Table 2) under the control of the *tac* promoter, forming the construct pKK223-OsALMT7.Then, the mutant stain CBT315 was transformed with the construct pKK223-OsALMT7. The empty vector (pKK223-3) was transformed into CBT315 as a negative control and into K-12 as a positive control. All strains were grown on M9 medium supplemented with 10 mM L-malic acid as the sole carbon source (pH adjusted to 6.6 with NaOH) at 37°C for 3 d. To confirm OsALMT7 expression in the CBT315 strain, immunoblotting was performed using standard protocols with anti- OsALMT7 antisera (Abmart; 15222), and the signal was detected by an enhanced HRP-DAB substrate kit (PA110; Tiangen).

In Vitro Transcription and Expression in *Xenopus laevis* Oocytes

For functional analysis in oocytes, the coding sequences of *OsALMT7*, *paab1-t1*, and *paab1-t2* were cloned into the pGEMHE vector (Liman et al., 1992). The cRNAs were prepared in vitro using the T7 RiboMAX large-scale production system (Promega). Oocytes were isolated and maintained in the ND96 solution prior to the injections. The oocytes were injected with or without (control) 25 ng of cRNA in 50 nL water and incubated at 17°C in a modified Barth's solution containing 88 mM NaCl, 1.0 mM KCl, 0.91 mM $CaCl_2$, 0.33 mM $Ca(NO_3)_2$, 0.82 mM $MgSO_4$, 2.4 mM $NaHCO_3$, and 10 mM HEPES-NaOH (pH 7.5). Electrophysiological experiments were performed 2 d after cRNA injection, as described previously (Xu et al., 2006).

Electrophysiological Measurements in *X. laevis* Oocytes

Whole-cell recordings from oocytes were performed under constant perfusion at room temperature (22°C) with a Gene-Clamp 500B amplifier (Axon Instruments) using the conventional two-electrode voltage-clamp technique. The recording electrodes were filled with 3 M KCl. The inward currents were recorded in oocytes that were preloaded with 50 nL water or 200 mM Na-malate. For the recording involved in different intracellular Na-malate concentrations, oocytes were injected with 50 nL of 100, 200, and 400 mM Na-malate to have intracellular Na-malate concentration of 8, 16, and 32 mM, respectively. The main bath solution consisted of 96 mM NaCl, 1.8 mM KCl, 1.8 mM $CaCl_2$, and 0.1 mM $LaCl_3$, with or without 0.1 mM $AlCl_3$ (pH 4.5). The holding potential was set to 0 mV and voltage test pluses were stepped between −180 and 0 mV (in 10 mV increments). The bath solutions used for outward current recording and anion selectivity experiment contained 25 mM NaCl, 25 mM $NaNO_3$, 25 mM Na_2SO_4, 25 mM Na-malate, or Na-fumarate, added to the same solution (100 mM Na-gluconate, 100 mM Ca-gluconate, 100 mM Mg-gluconate, 100 mM K-gluconate, and 10 mM MES, pH 4.5). The voltage test pluses were stepped between 0 and 100 mV (in 10-mV increments). The current-voltage (I/V) relationships were constructed by measuring the current amplitude at the end of test pulses. Reversal potential of oocytes expressing *OsALMT7* was measured in bath solutions with 1, 10, 25, or 50 mM malate, after preloading with 46 nL of 100 mM malate in oocytes. Reversal potential was valued through cross

points of the I-V curves and *x* axes (I = 0). In addition, inside-out single-channel recording in oocytes was performed following the method (Maksaev and Haswell, 2015). The pipette solution contains 25 mM malate, 5 mM Mg-gluconate, 0.5 $MgCl_2$, 10 mM MES/Tris (pH 7.2), and D-mannitol (Π = 220 mosmol kg^{-1}). The bath solution contains 35 mM malate, 5 mM Mg-gluconate, 0.5 $MgCl_2$, 10 mM MES/Tris (pH 7.2), and D -mannitol (Π = 220 mosmol kg^{-1}).

Malate Content Analysis

For malate transport assay, 5-d-old seedlings were transferred into a hydroponic solution containing 0 or 0.3 mM malate and treated for 24 h. The roots and shoots were collected and rinsed three times with deionized water. Malate content was measured according to a previously described enzymatic method (Delhaize et al., 1993). Briefly, samples (0.2 g fresh weight) obtained from seedlings after malate treatment and panicles at different elongation stages were homogenized in 3 mL water and incubated at 75°C for 15 min. After centrifugation, 0.2 mL of the supernatant was taken and mixed with 2.4 mL buffer (0.1 M glycine, 0.1 M glutamate, 2 mM NAD, and 2 μL of 1KU GOT). Then, the mix was preincubated for 10 min to obtain a stable absorbance reading at 340 nm, followed by addition of 5 μL 5KU malate dehydrogenase to activate the reaction for 10 min. The absorbance readings before and after the addition of malate dehydrogenase were recorded and used for calculation of NADH production and malate content. The malate content analysis was performed with three independent replicates and each sample included five plants.

Nitrate Content Analysis

Nitrate contents in different portions of panicles were determined according to the salicylic acid method (Vendrell and Zupancic, 1990). Specifically, samples (0.1 g fresh weight) were frozen with liquid nitrogen, ground to powder, and then suspended in 1 mL of deionized water, followed by boiling at 100°C for 20 min. After centrifugation at 15,000*g* for 10 min, 0.1 mL supernatant was transferred into a new tube. Then, 0.4 mL of salicylic acid-sulfate acid (5 g salicylic acid in 100 mL sulfate acid) was added into the tube. After thorough mixing, the reactions were incubated at room temperature for 30 min, and then 9.5 mL of 8% NaOH solution was added. The reaction was cooled down to room temperature before the absorbance was measured at 410 nm. Nitrate concentration was determined according to a standard curve made with KNO_3 at concentrations between 10 and 100 mg/L. Finally, the nitrate content in samples was calculated using the following equation: Y = CV/W (Y, nitrate content; C, nitrate concentration; V, total volume of extracted sample; W, weight of sample). The nitrate content analysis was performed with three independent replicates and each sample included five plants.

Malate Injections to Developing Panicles

Field-grown wild-type and *paab1-1* plants were used for the malate injection experiments. First, tillers of the wild-type plants with panicles at approximately the 7-cm stage were tested by injecting either distilled water or 1.5 mM malate (pH 5.2) to examine if the injection method and exogenous supply of malate have any effect on growth of the young panicles. Injection to tillers was performed with a 1-mL plastic syringe at a site slightly above the top of a panicle. A volume of 0.5 mL was injected to each of the chosen tillers. Subsequently, the *paab1-1* tillers with panicles at either the 7- or 5-cm stage were injected with 0.5 mL of water or 3 and 6 mM malate, respectively, in the same way. In addition, sequential injections (4 d after the first injection) were applied to some of the tillers. Ten tillers were used for each treatment. When the treated panicles emerged out of the flag leaf sheaths, the spikelet abortion rate was calculated and then analyzed by the Student's *t* test.

Accession Numbers

Sequence data from this article can be found in the GenBank/EMBL databases under the following accession numbers: OsALMT7, AK108963; OsVPE2, AK067597; OsVPE3,AK070079; and UBIQUITIN, AK059011.

Supplemental Data

Supplemental Figure 1. Impaired Spikelet Growth and Reduced Grain Size in Middle Portion of the *paab1-1* Panicle.

Supplemental Figure 2. Degenerating Flower Organs in Top Spikelets of *paab1-1* Panicle.

Supplemental Figure 3. Scanning Electron Microscopy of Apical Spikelets in the Wild Type and *paab1-1* at Early Stages.

Supplemental Figure 4. Histological Analysis of Apical Spikelets in the Wild Type and *paab1-1*.

Supplemental Figure 5. Microscopic Observation of the Apical Spikelet Hulls from Panicles of Three Selected Developmental Stages.

Supplemental Figure 6. DNA Fragmentation in the *paab1-1* Apical Spikelets.

Supplemental Figure 7. Alignment of the Amino Acid Sequences of OsALMT7 in Wild-Type, *paab1-1*, and *paab1-2* mutants.

Supplemental Figure 8. Reverse-Transcription Quantitative PCR Analysis of *OsALMT7* and Mutant Transcripts in the Wild Type and *paab1-1* Mutant, Respectively.

Supplemental Figure 9. Characterization of the *OsALMT7* Allelic Mutant *paab1-2*.

Supplemental Figure 10. Phenotypic Observations of *OsALMT7*-RNAi Transgenic Lines in Four *japonica* Backgrounds.

Supplemental Figure 11. Relative Expression of *OsALMT7* Homologs in *OsALMT7* Knockdown Plants.

Supplemental Figure 12. Transmembrane Helix Prediction of OsALMT7.

Supplemental Figure 13. Phylogenetic Tree of ALMT Proteins.

Supplemental Figure 14. Promoter Activity Analysis of *OsALMT7* Using *GUS* as a Reporter.

Supplemental Figure 15. OsALMT7 Is Localized in the Plasma Membranes of Transgenic Rice and Onion Epidermal Cells.

Supplemental Figure 16. Plasma Membrane Localization and Functional Evaluation of the OsALMT7-GFP Fusion Protein.

Supplemental Figure 17. Inside-out Single Channel Currents from Oocytes Expressing *OsALMT7* and Water (Control) at Two Membrane Potentials.

Supplemental Figure 18. OsALMT7-Mediated Outward Currents Recorded from Oocytes.

Supplemental Figure 19. OsALMT7-Mediated Inward Currents Are Not Activated by Al.

Supplemental Figure 20. Al Sensitivity Is Not Changed in *paab1-1*.

Supplemental Figure 21. Nitrate Content Is Not Changed in the *paab1-1* Panicle.

Supplemental Figure 22. Injection of Malate to *paab1-1* Plants with Panicles at 7 cm Stage Did Not Alleviate the Apical Panicle Abortion.

Supplemental Table 1. Molecular Marker Primers Used in Map-Based Cloning.

Supplemental Table 2. Primers Used for Plasmid Construction and Functional Analysis

Supplemental Data Set 1. Text File of the Alignment Used for the Phylogenetic Analysis Shown in Supplemental Figure 13.

ACKNOWLEDGMENTS

We thank Weihua Wu (China Agricultural University) for help with electrophysiological experiments. This research was supported by the grants from the National Key Research and Development Program of China (2016YFD0100403), the National Transgenic Science and Technology Program (2016ZX0800938B), and the National Natural Science Foundation of China (91535302 and 31401466).

AUTHOR CONTRIBUTIONS

J.W. supervised the project. Z.C., C.W., and J.W. designed the research. Y.H., Y.L., S.L., J.C., and H.Z. performed research. Y.H., Y.L., J.M., and M.W. analyzed data. Z.C. provided the plant material. J.L., J.T., S.Z., Y.R., and C.W. provided technical assistance. C.L. and J.W. cultivated the transgenic plants in the field. X.Z. and X.G. generated the transgenic plants. Y.H. wrote the article. Z.C., C.W., and H.W. revised the article.

Received January 2, 2018; revised March 14, 2018; accepted April 1, 2018; published April 2, 2018.

REFERENCES

Ashikari, M., Sakakibara, H., Lin, S., Yamamoto, T., Takashi, T., Nishimura, A., Angeles, E.R., Qian, Q., Kitano, H., and Matsuoka, M. (2005). Cytokinin oxidase regulates rice grain production. Science **309:** 741–745.

Bai, J., et al. (2015). Rice *TUTOU1* encodes a suppressor of cAMP receptor-like protein that is important for actin organization and panicle development. Plant Physiol. **169:** 1179–1191.

Barbier-Brygoo, H., De Angeli, A., Filleur, S., Frachisse, J.M., Gambale, F., Thomine, S., and Wege, S. (2011). Anion channels/transporters in plants: from molecular bases to regulatory networks. Annu. Rev. Plant Biol. **62:** 25–51.

Bart, R., Chern, M., Park, C.J., Bartley, L., and Ronald, P.C. (2006). A novel system for gene silencing using siRNAs in rice leaf and stem-derived protoplasts. Plant Methods **2:** 13.

Chen, T.H., and Murata, N. (2002). Enhancement of tolerance of abiotic stress by metabolic engineering of betaines and other compatible solutes. Curr. Opin. Plant Biol. **5:** 250–257.

Cheng, Z.J., Mao, B.G., Gao, S.W., Zhang, L., Wang, J.L., Lei, C.L., Zhang, X., Wu, F.Q., Guo, X.P., and Wan, J. (2011). Fine mapping of *qPAA8*, a gene controlling panicle apical development in rice. J. Integr. Plant Biol. **53:** 710–718.

De Angeli, A., Zhang, J., Meyer, S., and Martinoia, E. (2013). AtALMT9 is a malate-activated vacuolar chloride channel required for stomatal opening in Arabidopsis. Nat. Commun. **4:** 1804.

Delhaize, E., Ryan, P.R., and Randall, P.J. (1993). Aluminum tolerance in wheat (*Triticum aestivum* L.) (II. Aluminum-stimulated excretion of malic acid from root apices). Plant Physiol. **103:** 695–702.

Delhaize, E., Gruber, B.D., and Ryan, P.R. (2007). The roles of organic anion permeases in aluminium resistance and mineral nutrition. FEBS Lett. **581:** 2255–2262.

Dellaporta, S., Wood, J., and Hicks, J. (1983). A plant DNA minipreparation: Version II. Plant Mol. Biol. Report. **1:** 19–21.

Deng, M., et al. (2011). Bcl-2 suppresses hydrogen peroxide-induced programmed cell death via *OsVPE2* and *OsVPE3*, but not via *OsVPE1* and *OsVPE4*, in rice. FEBS J. **278:** 4797–4810.

Durbak, A.R., Phillips, K.A., Pike, S., O'Neill, M.A., Mares, J., Gallavotti, A., Malcomber, S.T., Gassmann, W., and McSteen, P. (2014). Transport of boron by the tassel-less1 aquaporin is critical for vegetative and reproductive development in maize. Plant Cell **26:** 2978–2995.

Fernie, A.R., and Martinoia, E. (2009). Malate. Jack of all trades or master of a few? Phytochemistry **70:** 828–832.

Fu, J., Huang, Z., Wang, Z., Yang, J., and Zhang, J. (2011). Pre-anthesis non-structural carbohydrate reserve in the stem enhances the sink strength of inferior spikelets during grain filling of rice. Field Crops Res. **123:** 170–182.

Hiei, Y., and Komari, T. (2008). Agrobacterium-mediated transformation of rice using immature embryos or calli induced from mature seed. Nat. Protoc. **3:** 824–834.

Hodges, D.M., DeLong, J.M., Forney, C.F., and Prange, R.K. (1999). Improving the thiobarbituric acid-reactive-substances assay for estimating lipid peroxidation in plant tissues containing anthocyanin and other interfering compounds. Planta **207:** 604–611.

Hoekenga, O.A., et al. (2006). *AtALMT1*, which encodes a malate transporter, is identified as one of several genes critical for aluminum tolerance in Arabidopsis. Proc. Natl. Acad. Sci. USA **103:** 9738–9743.

Huang, X., Qian, Q., Liu, Z., Sun, H., He, S., Luo, D., Xia, G., Chu, C., Li, J., and Fu, X. (2009). Natural variation at the DEP1 locus enhances grain yield in rice. Nat. Genet. **41:** 494–497.

Ikeda, K., Sunohara, H., and Nagato, Y. (2004). Developmental course of inflorescence and spikelet in rice. Breed. Sci. **54:** 147–156.

Ikeda, K., Nagasawa, N., and Nagato, Y. (2005). *ABERRANT PANICLE ORGANIZATION 1* temporally regulates meristem identity in rice. Dev. Biol. **282:** 349–360.

Ikeda, K., Ito, M., Nagasawa, N., Kyozuka, J., and Nagato, Y. (2007). Rice *ABERRANT PANICLE ORGANIZATION 1*, encoding an F-box protein, regulates meristem fate. Plant J. **51:** 1030–1040.

Ikeda-Kawakatsu, K., Maekawa, M., Izawa, T., Itoh, J., and Nagato, Y. (2012). *ABERRANT PANICLE ORGANIZATION 2/RFL*, the rice ortholog of Arabidopsis *LEAFY*, suppresses the transition from inflorescence meristem to floral meristem through interaction with *APO1*. Plant J. **69:** 168–180.

Itoh, J., Nonomura, K., Ikeda, K., Yamaki, S., Inukai, Y., Yamagishi, H., Kitano, H., and Nagato, Y. (2005). Rice plant development: from zygote to spikelet. Plant Cell Physiol. **46:** 23–47.

Jefferson, R. (1987). Assaying chimeric genes in plants: The *GUS* gene fusion system. Plant Mol. Biol. Report. **5:** 387–405.

Jeong, J., Suh, S., Guan, C., Tsay, Y.F., Moran, N., Oh, C.J., An, C.S., Demchenko, K.N., Pawlowski, K., and Lee, Y. (2004). A nodule-specific dicarboxylate transporter from alder is a member of the peptide transporter family. Plant Physiol. **134:** 969–978.

Jiao, Y., Wang, Y., Xue, D., Wang, J., Yan, M., Liu, G., Dong, G., Zeng, D., Lu, Z., Zhu, X., Qian, Q., and Li, J. (2010). Regulation of *OsSPL14* by OsmiR156 defines ideal plant architecture in rice. Nat. Genet. **42:** 541–544.

Kato, Y., Hirotsu, S., Nemoto, K., and Yamagishi, J. (2008). Identification of QTLs controlling rice drought tolerance at seedling stage in hydroponic culture. Euphytica **160:** 423–430.

Khush, G.S. (2000). New plant type of rice for increasing the genetic yield potential. In Rice Breeding and Genetics, J.S. Nanda, ed (Boca Raton, FL: Science Publishers), pp. 99–108.

Kobayasi, K., Yamane, K., and Imaki, T. (2001). Effects of Non-Structural Carbohydrates on Spikelet Differentiation in Rice. Plant Prod. Sci. **4:** 9–14.

Komatsu, K., Maekawa, M., Ujiie, S., Satake, Y., Furutani, I., Okamoto, H., Shimamoto, K., and Kyozuka, J. (2003b). *LAX* and *SPA*: major regulators of shoot branching in rice. Proc. Natl. Acad. Sci. USA **100:** 11765–11770.

Komatsu, M., Maekawa, M., Shimamoto, K., and Kyozuka, J. (2001). The *LAX1* and *FRIZZY PANICLE 2* genes determine the inflorescence architecture of rice by controlling rachis-branch and spikelet development. Dev. Biol. **231:** 364–373.

Komatsu, M., Chujo, A., Nagato, Y., Shimamoto, K., and Kyozuka, J. (2003a). *FRIZZY PANICLE* is required to prevent the formation of axillary meristems and to establish floral meristem identity in rice spikelets. Development **130:** 3841–3850.

Kovermann, P., Meyer, S., Hörtensteiner, S., Picco, C., Scholz-Starke, J., Ravera, S., Lee, Y., and Martinoia, E. (2007). The Arabidopsis vacuolar malate channel is a member of the ALMT family. Plant J. **52:** 1169–1180.

Lee, H.K., Cho, S.K., Son, O., Xu, Z., Hwang, I., and Kim, W.T. (2009). Drought stress-induced Rma1H1, a RING membrane-anchor E3 ubiquitin ligase homolog, regulates aquaporin levels via ubiquitination in transgenic Arabidopsis plants. Plant Cell **21:** 622–641.

Lee, M., Choi, Y., Burla, B., Kim, Y.Y., Jeon, B., Maeshima, M., Yoo, J.Y., Martinoia, E., and Lee, Y. (2008). The ABC transporter AtABCB14 is a malate importer and modulates stomatal response to CO2. Nat. Cell Biol. **10:** 1217–1223.

Li, S., Qian, Q., Fu, Z., Zeng, D., Meng, X., Kyozuka, J., Maekawa, M., Zhu, X., Zhang, J., Li, J., and Wang, Y. (2009). *Short panicle1* encodes a putative PTR family transporter and determines rice panicle size. Plant J. **58:** 592–605.

Liman, E.R., Tytgat, J., and Hess, P. (1992). Subunit stoichiometry of a mammalian K^+ channel determined by construction of multimeric cDNAs. Neuron **9:** 861–871.

Lin, A., Wang, Y., Tang, J., Xue, P., Li, C., Liu, L., Hu, B., Yang, F., Loake, G.J., and Chu, C. (2012). Nitric oxide and protein S-nitrosylation are integral to hydrogen peroxide-induced leaf cell death in rice. Plant Physiol. **158:** 451–464.

Liu, J., Zhou, M., Delhaize, E., and Ryan, P.R. (2017). Altered expression of a malate-permeable anion channel, OsALMT4, disrupts mineral nutrition. Plant Physiol. **175:** 1745–1759.

Maksaev, G., and Haswell, E.S. (2015). Expressing and characterizing mechanosensitive channels in Xenopus oocytes. Methods Mol. Biol. **1309:** 151–169.

Martinoia, E., and Rentsch, D. (1994). Malate compartmentation: responses to a complex metabolism. Annu. Rev. Plant Physiol. Plant Mol. Biol. **45:** 447–467.

Mathieu, Y., Guern, J., Pean, M., Pasquier, C., Beloeil, J.C., and Lallemand, J.Y. (1986). Cytoplasmic pH regulation in *Acer pseudoplatanus* cells: II. Possible mechanisms involved in pH regulation during acid load. Plant Physiol. **82:** 846–852.

Meyer, S., De Angeli, A., Fernie, A.R., and Martinoia, E. (2010). Intra- and extra-cellular excretion of carboxylates. Trends Plant Sci. **15:** 40–47.

Meyer, S., Scholz-Starke, J., De Angeli, A., Kovermann, P., Burla, B., Gambale, F., and Martinoia, E. (2011). Malate transport by the vacuolar AtALMT6 channel in guard cells is subject to multiple regulation. Plant J. **67:** 247–257.

Miao, J., Guo, D., Zhang, J., Huang, Q., Qin, G., Zhang, X., Wan, J., Gu, H., and Qu, L.J. (2013). Targeted mutagenesis in rice using CRISPR-Cas system. Cell Res. **23:** 1233–1236.

Middleton, R.E., Pheasant, D.J., and Miller, C. (1996). Homodimeric architecture of a ClC-type chloride ion channel. Nature **383:** 337–340.

Miura, K., Ikeda, M., Matsubara, A., Song, X.J., Ito, M., Asano, K., Matsuoka, M., Kitano, H., and Ashikari, M. (2010). *OsSPL14* promotes panicle branching and higher grain productivity in rice. Nat. Genet. **42:** 545–549.

Nakagawa, M., Shimamoto, K., and Kyozuka, J. (2002). Overexpression of *RCN1* and *RCN2*, rice *TERMINAL FLOWER 1/CENTRORADIALIS* homologs, confers delay of phase transition and altered panicle morphology in rice. Plant J. **29:** 743–750.

Oikawa, T., and Kyozuka, J. (2009). Two-step regulation of LAX PANICLE1 protein accumulation in axillary meristem formation in rice. Plant Cell **21:** 1095–1108.

Piñeros, M.A., Cançado, G.M.A., and Kochian, L.V. (2008a). Novel properties of the wheat aluminum tolerance organic acid transporter (TaALMT1) revealed by electrophysiological characterization in Xenopus oocytes: functional and structural implications. Plant Physiol. **147:** 2131–2146.

Piñeros, M.A., Cançado, G.M., Maron, L.G., Lyi, S.M., Menossi, M., and Kochian, L.V. (2008b). Not all ALMT1-type transporters mediate aluminum-activated organic acid responses: the case of ZmALMT1-an anion-selective transporter. Plant J. **53:** 352–367.

Rao, M.V., Lee, H., Creelman, R.A., Mullet, J.E., and Davis, K.R. (2000). Jasmonic acid signaling modulates ozone-induced hypersensitive cell death. Plant Cell **12:** 1633–1646.

Saha, A., Sarkar, R.K., and Yamagishi, Y. (1998). Effect of time of nitrogen application on spikelet differention and degeneration of rice. Bot. Bull. Acad. Sin. **39:** 119–123.

Sasaki, T., Yamamoto, Y., Ezaki, B., Katsuhara, M., Ahn, S.J., Ryan, P.R., Delhaize, E., and Matsumoto, H. (2004). A wheat gene encoding an aluminum-activated malate transporter. Plant J. **37:** 645–653.

Sasaki, T., Mori, I.C., Furuichi, T., Munemasa, S., Toyooka, K., Matsuoka, K., Murata, Y., and Yamamoto, Y. (2010). Closing plant stomata requires a homolog of an aluminum-activated malate transporter. Plant Cell Physiol. **51:** 354–365.

Senanayake, N., De Datta, S.K., Naylor, R.E.L., and Tomson, W.J. (1991). Lowland rice apical development: stages and cultivar differences detected by electron microscopy. Agron. J. **83:** 1013–1023.

Sheehy, J.E., Dionora, M.J.A., and Mitchell, P.L. (2001). Spikelet numbers, sink size and potential yield in rice. Field Crops Res. **71:** 77–85.

Smith, A.M., and Stitt, M. (2007). Coordination of carbon supply and plant growth. Plant Cell Environ. **30:** 1126–1149.

Sweetman, C., Deluc, L.G., Cramer, G.R., Ford, C.M., and Soole, K.L. (2009). Regulation of malate metabolism in grape berry and other developing fruits. Phytochemistry **70:** 1329–1344.

Tabuchi, H., et al. (2011). *LAX PANICLE2* of rice encodes a novel nuclear protein and regulates the formation of axillary meristems. Plant Cell **23:** 3276–3287.

Tan, C.J., Sun, Y.J., Xu, H.S., and Yu, S.B. (2011). Identification of quantitative trait locus and epistatic interaction for degenerated spikelets on the top of panicle in rice. Plant Breed. **130:** 177–184.

Tanaka, W., Pautler, M., Jackson, D., and Hirano, H.Y. (2013). Grass meristems II: inflorescence architecture, flower development and meristem fate. Plant Cell Physiol. **54:** 313–324.

Van Breusegem, F., and Dat, J.F. (2006). Reactive oxygen species in plant cell death. Plant Physiol. **141:** 384–390.

Vendrell, P.F., and Zupancic, J. (1990). Determination of soil nitrate by transnitration of salicylic acid. Commun. Soil Sci. Plant Anal. **21:** 1705–1713.

Von Arnim, A. (2007). Subcellular localization of GUS- and GFP-tagged proteins in onion epidermal cells. Cold Spring Harb. Protoc. **2007:** pdb prot4689.

Wagner, C.A., Friedrich, B., Setiawan, I., Lang, F., and Bröer, S. (2000). The use of *Xenopus laevis* oocytes for the functional characterization of heterologously expressed membrane proteins. Cell. Physiol. Biochem. **10:** 1–12.

Wegner, L.H., and Zimmermann, U. (2004). Bicarbonate-induced alkalinization of the xylem sap in intact maize seedlings as measured in situ with a novel xylem pH probe. Plant Physiol. **136:** 3469–3477.

Wegner, L.H., Stefano, G., Shabala, L., Rossi, M., Mancuso, S., and Shabala, S. (2011). Sequential depolarization of root cortical and stelar cells induced by an acute salt shock - implications for Na(+) and K(+) transport into xylem vessels. Plant Cell Environ. **34:** 859–869.

Xicluna, J., Lacombe, B., Dreyer, I., Alcon, C., Jeanguenin, L., Sentenac, H., Thibaud, J.B., and Chérel, I. (2007). Increased functional diversity of plant K^+ channels by preferential heteromerization of the shaker-like subunits AKT2 and KAT2. J. Biol. Chem. **282:** 486–494.

Xing, Y., and Zhang, Q. (2010). Genetic and molecular bases of rice yield. Annu. Rev. Plant Biol. **61:** 421–442.

Xu, J., Li, H.D., Chen, L.Q., Wang, Y., Liu, L.L., He, L., and Wu, W.H. (2006). A protein kinase, interacting with two calcineurin B-like proteins, regulates K^+ transporter AKT1 in Arabidopsis. Cell **125:** 1347–1360.

Xu, M., Gruber, B.D., Delhaize, E., White, R.G., James, R.A., You, J., Yang, Z., and Ryan, P.R. (2015). The barley anion channel, HvALMT1, has multiple roles in guard cell physiology and grain metabolism. Physiol. Plant. **153:** 183–193.

Yamagishi, J., Miyamoto, N., Hirotsu, S., Laza, R.C., and Nemoto, K. (2004). QTLs for branching, floret formation, and pre-flowering floret abortion of rice panicle in a temperate japonica x tropical japonica cross. Theor. Appl. Genet. **109:** 1555–1561.

Yao, Y., Yamamoto, Y., Yoshida, T., Nitta, Y., and Miyazaki, A. (2000). Response of differentiated and degenerated spikelets to top-dressing, shading and day/night temperature treatments in rice cultivars with large panicles. Soil Sci. Plant Nutr. **46:** 631–641.

Ye, J., Wang, X., Hu, T., Zhang, F., Wang, B., Li, C., Yang, T., Li, H., Lu, Y., Giovannoni, J.J., Zhang, Y., and Ye, Z. (2017). An InDel in the promoter of*Al-ACTIVATED MALATE TRANSPORTER9* selected during tomato domestication determines fruit malate contents and aluminum tolerance. Plant Cell **29:** 2249–2268.

Yoshida, A., et al. (2013). *TAWAWA1*, a regulator of rice inflorescence architecture, functions through the suppression of meristem phase transition. Proc. Natl. Acad. Sci. USA **110:** 767–772.

Yoshida, A., Ohmori, Y., Kitano, H., Taguchi-Shiobara, F., and Hirano, H.Y. (2012). *Aberrant spikelet and panicle1*, encoding a TOPLESS-related transcriptional co-repressor, is involved in the regulation of meristem fate in rice. Plant J. **70:** 327–339.